ENVIRONMENTAL RESEARCH
ECOLOGY

PURPOSE-LED PUBLISHING™ Part of the ENVIRONMENTAL RESEARCH SERIES

PAPER • OPEN ACCESS

High-resolution canopy fuel maps based on GEDI: a foundation for wildfire modeling in Germany

To cite this article: Johannes Heisig *et al* 2025 *Environ. Res.: Ecology* **4** 015003

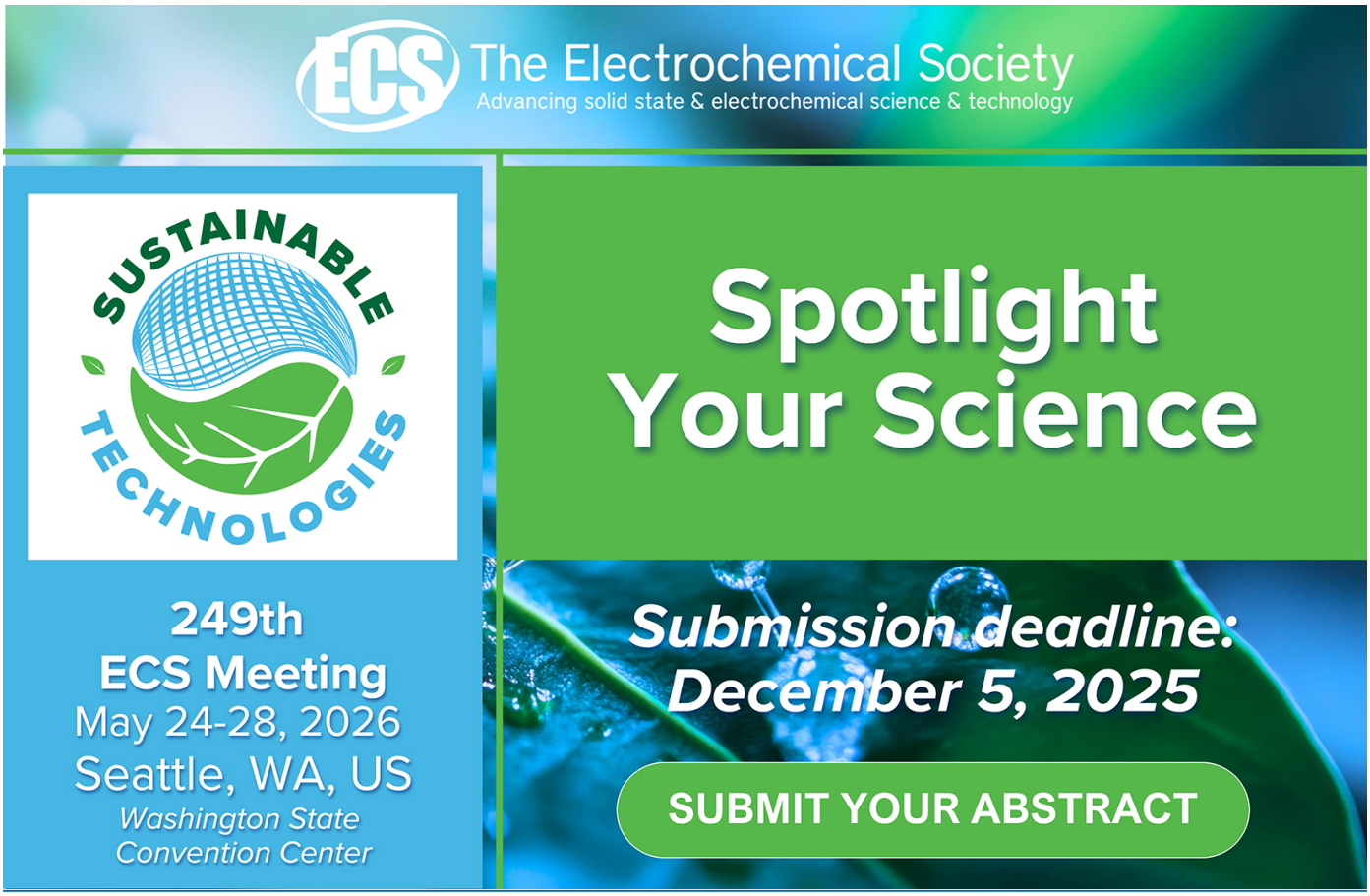

ENVIRONMENTAL RESEARCH
ECOLOGY

OPEN ACCESS

RECEIVED
3 September 2023

REVISED
13 January 2025

ACCEPTED FOR PUBLICATION
16 January 2025

PUBLISHED
24 January 2025

PAPER

High-resolution canopy fuel maps based on GEDI: a foundation for wildfire modeling in Germany

Johannes Heisig[1,*], **Milutin Milenković**[2] **and Edzer Pebesma**[1]

[1] Institute for Geoinformatics, University of Münster, Heisenbergstraße 2, 48149 Münster, Germany
[2] International Institute for Applied Systems Analysis, Schlossplatz 1, 2361 Laxenburg, Austria
[*] Author to whom any correspondence should be addressed.

E-mail: jheisig@uni-muenster.de

Keywords: GEDI, canopy, fuels, forest, wildfire, LiDAR, Germany

Abstract

Forest fuels are essential for wildfire behavior modeling and risk assessments but difficult to quantify accurately. An increase in fire frequency in recent years, particularly in regions traditionally not prone to fire, such as central Europe, has increased demands for large-scale remote sensing fuel information. This study develops a methodology for mapping canopy fuels over large areas (Germany) at high spatial resolution, exclusively relying on open remote sensing data. We propose a two-step approach where we first use measurements from NASA's Global Ecosystem Dynamics Investigation (GEDI) instrument to estimate canopy fuel variables at the footprint level, before predicting high-resolution raster maps. Instead of using field measurements, we generate (GEDI-) footprint-level estimates for canopy (Base) height (CH, CBH), cover (CC), bulk density (CBD), and fuel load (CFL) by segmenting airborne Light Detection and Ranging point clouds and processing tree-level metrics with allometric crown biomass models. To predict footprint-level canopy fuels we fit and tune Random Forest models, which are cross-validated using *k*-fold nearest neighbor distance matching. Predictions at >1.6 M GEDI footprints and biophysical raster covariates are combined with a universal Kriging method to produce countrywide maps at 20 m resolution. Agreement ($RMSE/R^2$) with validation data (from the same population) was strong for footprint-level predictions and moderate for map predictions. A validation with estimates based on National Forest Inventory data revealed low to modest agreement. Better accuracy was achieved for variables related to height (CH, CBH) rather than to cover or biomass (CBD, CFL). Error analysis pointed towards a mixture of biases in model predictions and validation data, as well as underestimation of model prediction standard errors. Contributing factors may be simplification through allometric equations and spatial and temporal mismatch of data inputs. The proposed workflow has the potential to support regions where wildfire is an emerging issue, and fuel and field information is scarce or unavailable.

1. Introduction

Central Europe is exposed to a growing number of extreme drought events and heat waves induced by climate change (IPCC 2014). As a result, tree canopy mortality has recently increased (Senf *et al* 2018, Thonfeld *et al* 2022). Susceptibility to biotic and abiotic disturbances grows as forest health declines (Schuldt *et al* 2020). Hence, bark beetles, fungi, storms, or fire can further impact the resilience of forest ecosystems. Whilst European temperate forests have mostly been spared of wildfire in the past, they are now expected to face more and larger fire events (Seidl *et al* 2014, Cardil *et al* 2021). Symptoms of this trend were observed during Germany's fire seasons in 2018 and 2019 (BMEL 2018, 2019), fueling the discussion of fire prevention, climate change adaptation, and mitigation. With wildfires becoming a frequent challenge in the near future, decision-makers need to be informed of vulnerable stands. Quantifying wildfire fuels is a crucial component in the assessment of potential hazards and risks.

Canopy (or crown) fuel variables describe aerial biomass and structure of typically trees or shrubs (Keane *et al* 2001). We consider five canopy fuel variables relevant to fire behavior modeling in this study: canopy height (CH, [m]) defined as the top height of the tree canopy; canopy base height (CBH, [m]) defined as the height of the lowest fire-propagating fuel particle (branches, leaves, needles) of a tree; canopy cover (CC, [%]) defined as portion of the ground covered by the vertical projection of the canopy; canopy fuel load (CFL, [t ha^{-1}]) defined as the available canopy fuel per unit area; and crown bulk density (CBD, [kg m^{-3}]) defined as the mass of CFL per unit volume (Jennings *et al* 1999, Chuvieco *et al* 2003, Hermosilla *et al* 2014). Available canopy fuel is defined as the proportion of total canopy fuel ('foliage and a small fraction of branchwood') that burns under given conditions, e.g. moisture level (Scott and Reinhardt 2001).

Individual canopy fuel variables influence fire behavior differently. CH affects wind dynamics and ember travel range in torching (Finney 1998). CC also regulates wind speed in addition to limiting the amount of light that reaches lower vertical forest strata and thereby controlling understory growth and surface fuel moisture (Jennings *et al* 1999, Chuvieco *et al* 2003). CBH affects a surface fire's potential to reach the canopy, while CFL and CBD determine the crown fire intensity and spread rate (Finney 1998, Chuvieco *et al* 2003).

Operational fire management requires fuels information to have four key properties: (a) large spatial coverage, (b) high spatial detail, (c) high update frequency, and (d) high accuracy (Keane *et al* 2001). Yet, great diversity and spatio-temporal variability of wildfire fuels pose challenges for their quantification (Erdody and Moskal 2010, Keane *et al* 2012). Most fuels mapping approaches do not fulfill all of these requirements simultaneously.

Experienced forestry professionals may measure vegetation properties most accurately (Arroyo *et al* 2008), but inventory campaigns are spatially limited and repeated infrequently (Chuvieco *et al* 2003). Indirect estimation methods are more popular as higher spatio-temporal field sampling frequency is too costly (Erdody and Moskal 2010).

Remote sensing methods enable consistent fuels assessments with large spatial coverage and reasonable temporal resolution (Riaño 2003). Their repeated acquisitions mark a substantial advantage over field measurements. Optical imagery is accessible at a high spatio-temporal resolution but has been found to encounter signal saturation problems when used to map vertical structure (Healey *et al* 2020, Potapov *et al* 2021). Further, single- and multi-layer canopies cannot be separated in optical data but may have implications, e.g. for fuel load. Synthetic aperture radar (SAR) sensors are superior to optical sensors in that they can penetrate forest canopies and clouds while having similar spatial resolution and improved temporal sampling. They have proven to provide insight into forest structure (Dostálová *et al* 2016) and above-ground biomass (Berninger *et al* 2018). Even though many satellite sensors fulfill spatial and temporal resolution and coverage requirements for assessing fuels, mapping the third (vertical) dimension from space with high precision remains difficult.

Light Detection and Ranging (LiDAR) can measure vegetation structure either by collecting (a) discrete returns, i.e. point clouds, or (b) waveforms, i.e. vertical distribution of laser energy reflected by vegetation. The high density of discrete returns and small footprint size generated by LiDAR aircraft sensors ensure reliable sampling of the vegetation structure and a better chance of intersecting ground, understory, or branchwood through canopy gaps. This is especially important in almost closed or multi-story canopies. Tree-level data may be collected after identifying individual specimen through point cloud segmentation (Parkan and Tuia 2018). Despite its widely acknowledged effectiveness, small aircraft LiDAR data campaigns are expensive, spatially limited, and, therefore, infrequently updated. Secondly, waveform LiDAR sensors integrate return energy over a larger footprint, and its distribution reflects vertical vegetation structure (Dubayah *et al* 2020). Spaceborne waveform LiDAR systems like the Global Ecosystem Dynamics Investigation (GEDI) instrument pick up fewer details than airborne discrete LiDAR. In addition, the sparse sampling design of footprint measurements does not allow for directly deriving high-resolution maps. Their advantage, however, lies in the near-global coverage, making it appropriate for large-scale, e.g. country-level mapping efforts (Duncanson 2022).

Canopy fuel predictions with a high level of spatial detail were produced by multiple studies that used small-footprint discrete-return airborne LiDAR data (Riaño 2003, Andersen *et al* 2005, Erdody and Moskal 2010, Hermosilla *et al* 2014, Hudak *et al* 2016, Chamberlain *et al* 2021). The LANDFIRE project provides datasets relevant to wildfire modeling in the US at 30 m spatial resolution (Rollins 2009). It achieves its large coverage by combining Landsat imagery with plot-level estimates obtained through the National Forest Inventory (NFI) program. As multi-spectral and LiDAR data complement each other in describing vegetation properties, their combination has improved predictive models for landscape-scale fuels mapping (Arroyo *et al* 2008, Erdody and Moskal 2010, García *et al* 2017, Chuvieco *et al* 2020). While many fuel studies focus on fire-prone North America, similar methods have been applied in the Mediterranean region (Marino *et al* 2016, Sánchez Sánchez *et al* 2018) and in Central Europe (Taccaliti *et al* 2021, Heisig *et al* 2022). The value of GEDI data for assessing forest structure and canopy fuels was recently investigated. Kacic *et al* (2023)

modeled CH, CC, and above-ground biomass density (AGBD) in Germany and its dynamics between 2017 and 2022 using GEDI, airborne LiDAR and Sentinel-1 & -2 data. Leite *et al* (2022) predicted fuel type grids at 1 km spatial resolution for the Cerrado biome in Brazil using simulated GEDI waveforms and airborne LiDAR. Hoffrén *et al* (2023) classified fuel types in north-eastern Spain by feeding GEDI and Landsat-8 data into a machine learning (ML) model. Outside the wildfire context, two studies have recently created global tree height maps based on GEDI observations. Potapov *et al* (2021) fused GEDI data with Landsat time series in an ML regression model. Lang *et al* (2022) combined GEDI with Sentinel-2 imagery in a Deep Learning framework to generate an even finer global tree height product.

A vast majority of canopy fuel studies in the literature focus on the demonstration of methods and produce maps for small areas where high-quality field or LiDAR data are available. This is especially true for more challenging canopy fuel parameters like CBD or CBH, which require more assumptions and data processing steps than, e.g. CH or CC. When predicting fuels for large areas such as regions or countries, the majority of research produces coarse spatial data unsuitable for fine-grained fire behavior assessments (Lanorte *et al* 2001, Pettinari and Chuvieco 2016, Leite *et al* 2022). Regardless of coverage and resolution, fuels mapping efforts to this date rely on ground truth from physical sampling in the field. As field data does not exist or are not openly available in many countries, there is a need for a methodology that combines the advantages of various remote sensing data sources to map canopy fuels.

The aim of this study is to produce high spatial resolution (20 m) maps for five forest canopy fuel variables in Germany, relying on open and accessible data. It is noted that traditional approaches use field data to calibrate remote sensing data for creating predictions. Since forest inventory data are not open in our study case, we use widely available and accurate 3D airborne LiDAR measurements and well-established allometric models as proxies for field data on forest canopy fuel variables. The suggested methodology benefits from its extensive spatial coverage of airborne LiDAR acquisitions to train data-demanding ML canopy fuel prediction models. Furthermore, we introduce a two-step methodology, which predicts first the canopy fuels at the footprint-level, i.e. on GEDI observations, and then predicts the canopy fuel raster maps relying on a well-established geostatistical Kriging method and biophysical covariates. Footprint-level prediction models are cross-validated under a strict training-testing framework, whereas maps are validated with canopy fuel estimates based on NFI data. The final high-resolution canopy fuel maps thereby fill a data gap in the current Central European wildfire research and provide the basis for further risk and hazard assessments at all spatial scales.

2. Data

Our study considers GEDI waveform LiDAR measurements covering a larger part of Germany, freely available airborne LiDAR point cloud data from multiple federal states, satellite data covering the entire study area, and NFI measurements as validation data (see figure 1).

2.1. GEDI

GEDI is a relatively new spaceborne waveform LiDAR sensor onboard the International Space Station (ISS) operated by NASA. It measures vegetation structure inside footprints with a diameter of 25 m (Beck *et al* 2021) to infer, e.g. above-ground biomass (Dubayah *et al* 2020, Duncanson 2022). Following the ISS' orbit its observations are limited to 51.6° N/S, excluding a large part of northern Germany. The absence of data in this area bears challenges when predicting maps at the country-level. We use Level 2A canopy height metrics (Dubayah *et al* 2021a) and Level 2B canopy profile metrics (Dubayah *et al* 2021b) of GEDI version 2 data. The products are reported to have a mean 1-sigma horizontal geolocation error of 10.3 m (Beck *et al* 2021).

To access and filter GEDI Level 2A and 2B feature collections, we used Google Earth Engine (GEE) (Gorelick *et al* 2017) with collection IDs '`LARSE/GEDI/GEDI02_A_002/GEDI02_A(B)_*_V002`'. Observations were included if acquired by power beams during night time, if not flagged due to quality or degradation issues, if the relative height of the 98th height percentile (*rh98*) was between 2 and 60 m, and if sensitivity was above 0.95. Additionally, a forest mask was applied to exclude any non-forest vegetation observations. We computed the mask in GEE directly using ESA's World Cover product at 10 m resolution (Zanaga *et al* 2021), with a negative buffer of 50 m applied to compensate for the GEDI geolocation and edge errors. This way we sampled 1626 086 observations from 678 overpasses between April 2019 and December 2022. Appendix table A1 lists all GEDI metrics used in this analysis.

2.2. Open airborne LiDAR data

Since GEDI geolocation and height errors are at least one order of magnitude larger than airborne LiDAR errors (meter vs. dm to cm, respectively), airborne LiDAR is considered here as a reference dataset. Due to different data access policies among German federal states we were not able to derive canopy fuel maps based

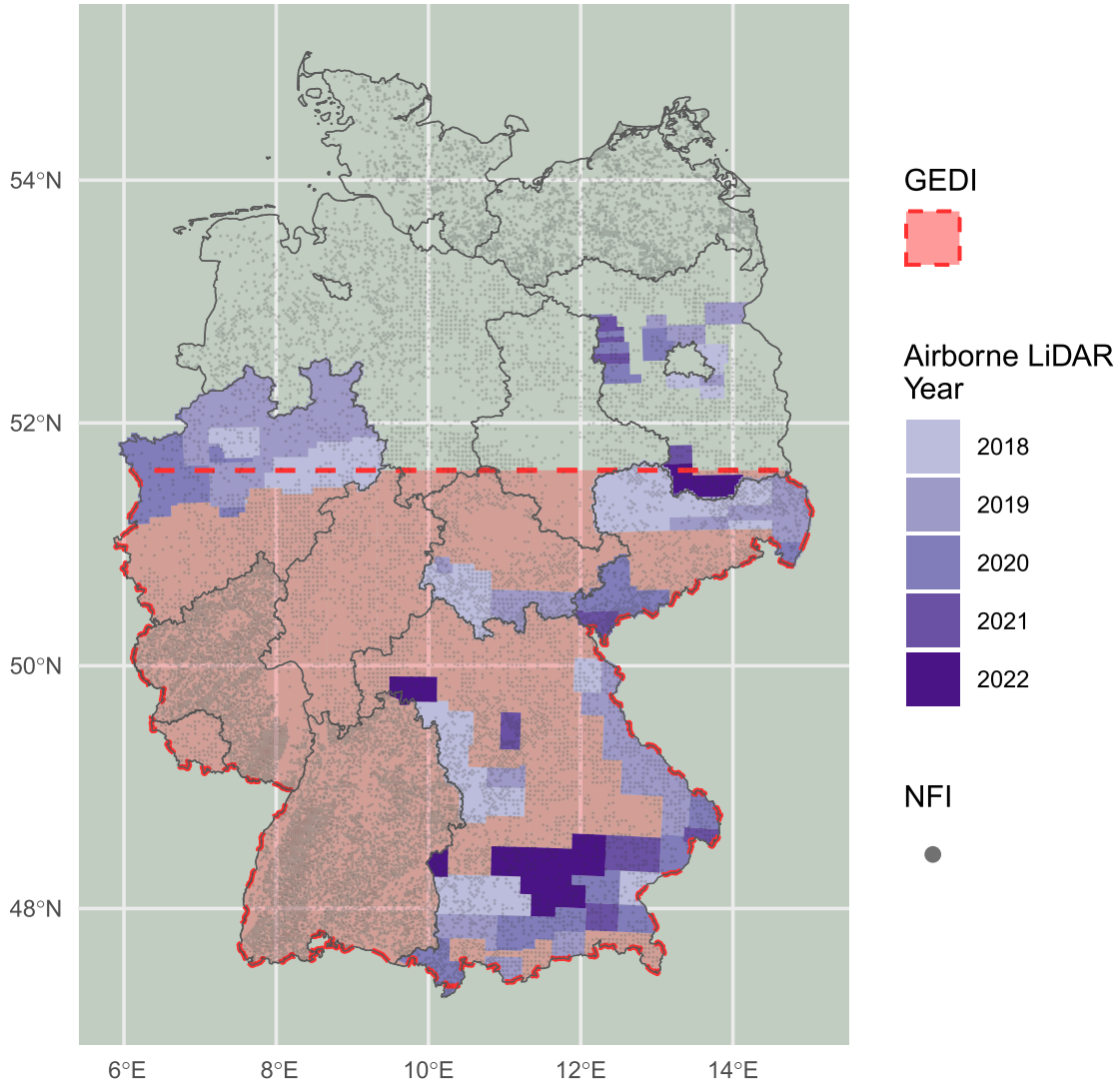

Figure 1. Spatial coverage of data used in this study. GEDI's extent reaches up to 51.6° N (within red dashed bounds). Open Airborne LiDAR data with acquisitions after GEDI's launch in 2018 exist in five German federal states. National Forest Inventory (NFI) data serve as reference for canopy fuel predictions. Each grey dot represents the approximate location of up to four NFI ground plots.

Table 1. List of airborne LiDAR data acquisitions from five German states used in this study. Data are characterized by minimum point density and horizontal and vertical measurement accuracy. Point density may be higher in vegetated areas as multiple returns can be detected from a single shot.

State	Min. Density ($pts\,m^{-2}$)	Accuracy (cm)		Source
		horizontal	vertical	
Bavaria	4	10	50	LDBV (2023)
Brandenburg	5	30	—	LGB (2023)
Northrhine-Westphalia	4	15	30	Geobasis NRW (2023)
Saxony	4	15	30	GeoSN (2023)
Thuringia	4	15	30	GDI Thüringen (2023)

on airborne LiDAR for the entire country, but had to fall back on GEDI. We obtained airborne LiDAR data from Northrhine-Westphalia, Thuringia, Saxony, Brandenburg, and Bavaria. Point density and spatial accuracy are presented in table 1. Data are provided with a classification dividing ground from non-ground returns. Yet, sensor type, number of returns and other mission specifications vary among federal states.

2.3. NFI

We accessed German NFI data from 2012 as the most recent publicly available inventory (BMEL 2016), collected and administered by the Thünen Institute for Rural Areas, Forestry and Fisheries. It includes

tree-level species labels and measurements related to vertical structure of over 500 000 individual trees at over 50 000 plot locations. These sets of measurements are hereinafter referred to as tree lists. Despite being a promising training dataset for spatial prediction tasks, German NFI data cannot be used for this purpose due to privacy regulations. While tree lists are publicly available, the exact coordinates of corresponding NFI plots are not, preventing the pairing with spatial covariate data. A validation of our final map products with canopy fuel estimates based on NFI data was only possible through direct collaboration with the administering institute. Thus, it is noted that German NFI data is only used for validation of the final products, not for model training.

2.4. Raster covariates

To predict canopy fuels at the country level, we collected 92 covariate raster maps from satellite acquisitions or derived biophysical variables. Datasets available as time series were reduced using three value (10th, 50th, and 90th) percentiles over the reference time frame of 2018. This approach aims at better covering the value range throughout the annual phenological cycle. An overview of all raster covariates is presented in appendix table A2.

The European Digital Elevation Model (EU-DEM, version 1.1) is provided by the Copernicus Land Monitoring Service (CLMS) and has a spatial resolution of 25 m (EU, CLMS, EEA 2023). Next to elevation we derived the terrain variables slope and aspect using the *terra* R-package (Hijmans *et al* 2022).

Blickensdörfer *et al* (2022) mapped the 11 most common dominant tree species in Germany at 10 m spatial resolution. The majority of forested area is therein attributed to spruce, pine, beech and oak. Minor classes are larch, fir, Douglas fir, birch, alder, and other deciduous species with high (ODH) and low (ODL) life expectancy. The authors used a Random Forests (RF) classification algorithm based on Sentinel-1 and -2 time series with NFI data serving as ground truth. The dataset is an important covariate in this study as vertical structure and growth form differ among tree species (Ø rka *et al* 2013).

We accessed the Sentinel-1 GEE image collection (‘`COPERNICUS/S1_GRD`’) with backscatter coefficient (sigma 0) values for polarization bands VH and VV and added their ratio (VV/VH) as a new band. All available acquisitions for 2018 were then pre-processed following a workflow proposed by Mullissa *et al* (2021), which applies border noise correction, speckle filtering and radiometric terrain normalization. After grouping the image collection by band and orbit (ascending/descending) we reduced each group to annual (radiometrically-terrain-corrected) backscatter images showing the 10th, 50th, and 90th value percentiles. Additional gray level co-occurrence matrix (GLCM) texture (Haralick *et al* 1973) was computed for the VV/VH ratio band using the *GLCMTextures* R-package (Ilich 2020) with a moving window size of three by three pixels. Metrics included contrast, dissimilarity, homogeneity, Angular Second Moment (ASM), entropy, mean, variance, and correlation.

Temporal composites from Sentinel-2 surface reflectance values and derived spectral indices for 2018 were computed in GEE. We filtered the Sentinel-2 image collection (‘`COPERNICUS/S2_SR`’) for scenes from 2018 with less than 5% cloud cover, masked remaining clouds with a simple procedure based on the quality assessment (QA) band and selected bands 1-8, 8A, 11, and 12. In addition to plain band values we added five spectral indices using the *spectral* library (Montero *et al* 2022): Normalized Difference Vegetation Index (NDVI), Enhanced Vegetation Index (EVI), EVI2, Normalized Difference Water Index (NDWI), and Soil-Adjusted Vegetation Index (SAVI). Each band or index time series was reduced to three new datasets by calculating the 10th, 50th, and 90th percentile.

We accessed six vegetation phenology parameters for 2018 based on 10 m Sentinel-2 data (EU, CLMS, EEA 2023), which are hosted on the WEkEO cloud processing platform. This product is derived from the Plant Phenology Index (PPI) and describes yearly vegetation development. Start, end, and length of the growing season, minimum and maximum PPI values, and total productivity where selected for this study.

As a second radar dataset we used the global mosaic for 2018 (version 2) acquired by L-band SAR (PALSAR-2) sensor on the Advanced Land Observing Satellite 2 (ALOS-2). Data were processed by JAXA and accessed via GEE (‘`JAXA/ALOS/PALSAR/YEARLY/SAR_EPOCH`’). Mosaics have undergone ortho-rectification, radiometric slope correction, and backscatter normalization (Shimada *et al* 2014).

Next to phenology we included leaf traits (Moreno-Martínez *et al* 2018), consisting of specific leaf area (SLA), leaf dry matter content (LDMC), leaf nitrogen (LNC) and phosphorus (LPC) content per dry mass, and leaf nitrogen/phosphorus ratio (LNPR). Traits were predicted using ML models and MODIS and Landsat data at 500 m pixel size.

As a promising predictor for canopy fuel load, we selected the above-ground biomass product for 2018 (version 3) from ESA’s Climate Change Initiative (CCI) (Santoro and Cartus 2021). This data is derived from

radar satellite observations and describes the oven-dry mass (t ha^{-1}) of tree stems, branches, and twigs with a spatial resolution of 100 m.

All raster covariates were warped to a common 20 m grid and projected to the European Terrestrial Reference System 1989 (ETRS89, EPSG 3035). The categorical species data were resampled using the mode statistic, while the mean was applied to all numerical rasters.

3. Methods

Our approach generates footprint-level estimates of five canopy fuel variables before using them to predict raster maps. Instead of performing field measurements, we derived synthetic tree lists from airborne LiDAR point clouds at the locations of GEDI observations (hereafter referred to as footprints). Each synthetic tree list produces one footprint-level canopy fuel estimate, which can be linked to GEDI metrics. We tested two statistical models (linear regression and RF) to utilize this relationship and predict canopy fuels at all available GEDI footprints. In a second step, universal Kriging (Pebesma and Bivand 2023) is applied to predict the desired variables in space using previously generated footprint-level estimates as training data. See figure 2 for a visualization of the modeling workflow. The details of each step are explained in the subsections below.

3.1. Spatio-temporal matching of GEDI and airborne LiDAR data

After collecting over 1.6 M GEDI footprints we matched them spatially and temporally with openly available airborne LiDAR point cloud tiles from five German states, which serve as training data. We established data requirements to ensure data homogeneity in space and time and produce high-quality reference data for the following modeling effort. Observations were selected if they intersected LiDAR tiles and filtered for instances where the difference in acquisition dates of GEDI and airborne LiDAR did not exceed 30 days. The matching process resulted in 8500 suitable footprints.

3.2. Footprint-level estimates based on airborne LiDAR data

Tree-level metrics required by allometric crown biomass equations include species, CH, CBH, diameter at breast height (DBH), crown class, and stem density. Together these data describe forest structure at the footprint-level (tree lists). We processed discrete-return LiDAR point clouds to directly derive or infer these metrics at the tree level (which is usually achieved through field measurements), to obtain synthetic tree lists.

Airborne LiDAR point clouds were clipped by applying a 12.5 m radius around the center of each GEDI footprint. Vertical measurement values were normalized by subtracting elevation. For this step the ground surface was derived through Kriging interpolation using the 40 Nearest Neighbors for each ground return. Individual trees were segmented from the point cloud by utilizing a growing region segmentation method introduced by Li *et al* (2012). For each tree we calculated CH as maximum of all height values and CBH as the maximum height of the 5% bin that shows the largest difference between lower and higher end of the bin, following Chamberlain *et al* (2021). Species labels where extracted from a raster classification product at 10 m spatial resolution (Blickensdörfer *et al* 2022). A Chi-squared test comparing the species label distributions of synthetic and NFI tree lists suggested no independence ($p < 0.0001$).

Tree-level DBH was inferred by leveraging the relationship between stem circumference and CH. Using NFI tree lists, we built simple linear regression models for each of the 11 tree species with CH being the only predictor. Tree-level DBH was then predicted by applying the models to LiDAR-derived CH.

Crown classes refer to a tree's vertical position in the canopy. A tree crown may be *dominant*—crown extends above main canopy, *co-dominant*—crown is part of main canopy, or *suppressed*—crown is completely overtopped by other crowns (Lutes 2021). We deduced crown class by testing whether CH is within the standard deviation interval around the footprint-level CH mean. Trees within this interval were considered *co-dominant*. Trees exceeding the interval on the higher (lower) end were classified *dominant* (*suppressed*). A Chi-squared test comparing the crown class distributions of synthetic and NFI tree lists suggested no independence ($p < 0.0001$).

Synthetic tree lists containing a total of 153 855 individuals were fed into *FuelCalc*, a program designed to calculate plot-level canopy fuel parameters from forestry field data using species-specific allometric crown biomass equations (Reinhardt *et al* 2006). Such equations stem from extensive field measurements and have not yet been established for common Central European species. Allometric equations mainly depend on DBH and yield biomass estimates for six particle size classes: total crown, foliage, twigs (<0.6 cm), and branches (0.6–2.5 cm, 2.5–7.5 cm, >7.5 cm). For each of our 11 local species we selected a North American proxy species with similar vertical structure and fire behavior attributes. Appendix table A3 lists (proxy) species and the respective equation references.

We also tested how GEDI geolocation error influenced the canopy fuel predictions. A subset of 30 GEDI footprints per overpass was selected randomly and shifted to every position on a star-shaped grid with 5

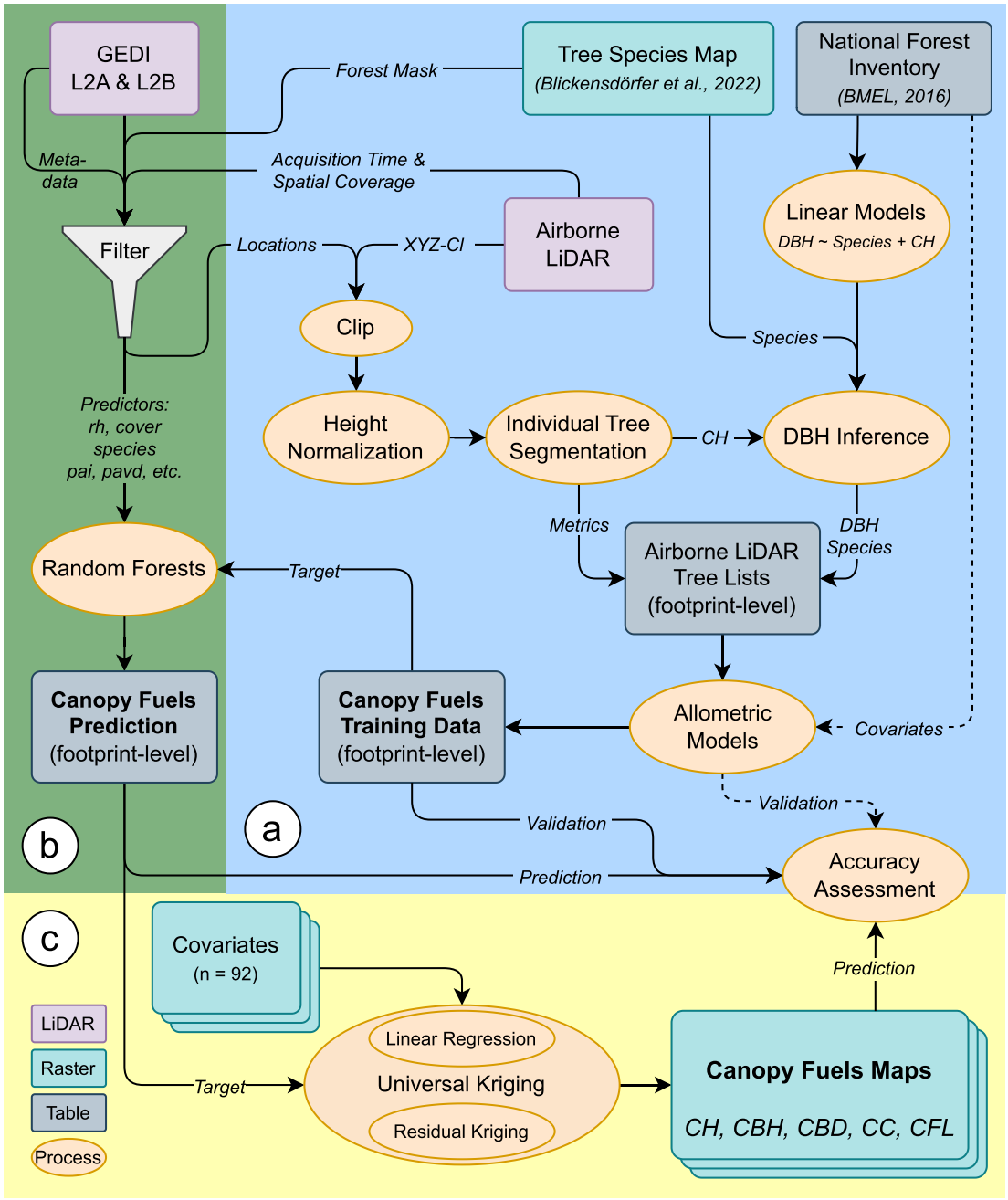

Figure 2. Canopy fuels modeling workflow: (a) footprint-level canopy fuel estimates are produced by segmenting airborne LiDAR point clouds, inferring tree-level properties to create synthetic tree lists, and applying allometric equations; (b) GEDI observations are filtered and serve as predictors for footprint-level canopy fuel estimates; (c) footprint-level estimates serve as basis for raster map predictions with a universal Kriging method. Footprint-level refers to the GEDI footprint (25 m diameter), not to airborne LiDAR.

steps (3–15 m) from the center in 8 directions deviating by a 45° angle from each other. The best shift (combination of angle and distance from the grid center) was calculated based on the smallest root mean squared error (*RMSE*) between the GEDI *rh98* values and the 1 m airborne CH model and then applied to all footprints from the respective overpass. However, we found that horizontally shifting GEDI footprint locations did not improve the performance of the subsequent modeling process, and thus, that step was finally omitted.

3.3. Footprint-level estimates based on GEDI data

We created a modeling dataset by pairing footprint-level canopy fuel outputs from *FuelCalc* with 25 m GEDI footprint-level measurements. As canopy structure is species-dependent (Bouvier *et al* 2015) we extracted the footprint-level species label (footprint center) as well as area fractions for each species from the 10 m species raster. This way a rough approximation of species composition was included in the analysis.

We built RF models for each of the five canopy fuel variables by keeping *ntrees* (number of decision trees) constant at 500. To find the best suitable set of hyperparameters we tuned *mtry* (number of splits at each branch) with values 5, 7, 9, 11, and 13 and *mns* (minimum size of a node after which no further splitting is allowed) with values 3, 5, and 7. To quantify variable importance we recorded impurity as the variance of the responses. The best sets for training final models were selected based on *RMSE* between test samples and model prediction, averaged over all *k* folds. Finally, canopy fuel variables were predicted at all remaining GEDI observations that were not included in the RF training process. It is noted that we also tested linear regression as a more simple alternative method, but RF outperformed it.

3.4. Map prediction

In a second modeling step, canopy fuel predictions at over 1.6 M GEDI footprints served as a basis for the prediction of raster maps. Here, the term map prediction refers to extending footprint-level estimates to all raster cells in the study area covered by forest based on covariates. This includes predictions within and beyond GEDI's acquisition range (>51.6° N). Map prediction was achieved with a universal Kriging approach, also known as *Kriging with External Drift* (Bivand *et al* 2008). Universal Kriging can be distinguished into two separate steps: first, a regression model is fitted using covariates and predicted at target locations; second, model residuals are interpolated in space through Kriging and added. We extracted raster covariates at GEDI footprints and built linear regression models with each of the five canopy fuel variables as dependent variables, respectively. RF regression models were tested but rejected because their accuracies did not exceed these of more simple linear models. Models were predicted onto raster covariates to obtain maps with a 20 m resolution covering Germany, but restrained to the forest mask applied to the tree species raster from Blickensdörfer *et al* (2022). All non-forest pixels had missing values. To consider spatial correlation in residual Kriging we calculated and fitted variogram models. Together with the GEDI footprints and raster covariates they acted as input to the Kriging algorithm, which was restricted to only consider the 100 Nearest Neighbors per target location. Linear model predictions and Kriging outputs were added up to a final map product.

3.5. Accuracy assessment

3.5.1. Footprint-level estimates

When evaluating the accuracy of maps predicted with statistical models the choice of a suitable cross-validation (CV) method is crucial. This choice should depend on the spatial sampling design, which affects geographic distances between training samples themselves and between training samples and prediction locations (Milá *et al* 2022). In order to yield robust map accuracy estimates, predictive conditions during CV and model prediction should match (Meyer and Pebesma 2022, Milá *et al* 2022, Ludwig *et al* 2023), meaning that the two distance distributions should be similar.

In case training data is a probability sample covering the entire prediction area, this condition is met (Baddeley *et al* 2016) and the use of traditional random (*k*-fold) CV can be justified (Wadoux *et al* 2021). For non-random sampling designs (e.g. clustered), where some regions are more strongly represented than others (De Bruin *et al* 2022), the condition is not met and random CV would result in too optimistic accuracy estimates. Training data in this study is collected along intersecting orbital flight tracks resulting in a strongly clustered sampling pattern (figure 3). It is further limited to boundaries of states providing open airborne LiDAR data, so that predictions are performed beyond the training area.

These circumstances induce higher requirements for accuracy assessment and call for a spatial CV approach (Meyer and Pebesma 2022). Multiple approaches have recently been developed and compared (Roberts *et al* 2017, Valavi *et al* 2019, De Bruin *et al* 2022, Milá *et al* 2022, Linnenbrink *et al* 2023, Mahoney *et al* 2023). Blocked CV methods use a regular grid and assign each training sample to a block which belongs to one of *k* CV folds (Roberts *et al* 2017, Valavi *et al* 2019). They can account for spatial auto-correlation and create independent folds if block size is chosen carefully, but may encounter challenges for strongly clustered samples (Roberts *et al* 2017). The nearest neighbor distance matching (NNDM) algorithm proposed by Milá *et al* (2022) modifies the conventional Leave-One-Out (LOO) CV approach to non-random sampling designs. For large training datasets, however, LOO CV is not computationally feasible. The enhanced kNNDM approach overcomes this issue by designing *k* folds such that empirical cumulative distribution functions (ECDF) of nearest neighbor distances between training and test samples and between training samples and prediction locations match (Linnenbrink *et al* 2023). For clustered samples the method has demonstrated more reliable accuracy estimates than other spatial CV methods (Linnenbrink *et al* 2023). Hence, we selected kNNDM as spatial CV method with $k = 10$ folds to best comply with GEDI's sampling pattern. Its effect on the distribution of Nearest Neighbor Distances is displayed in figure 4. While sample-to-sample distances differ strongly from sample-to-prediction distances, kNNDM folds offer a

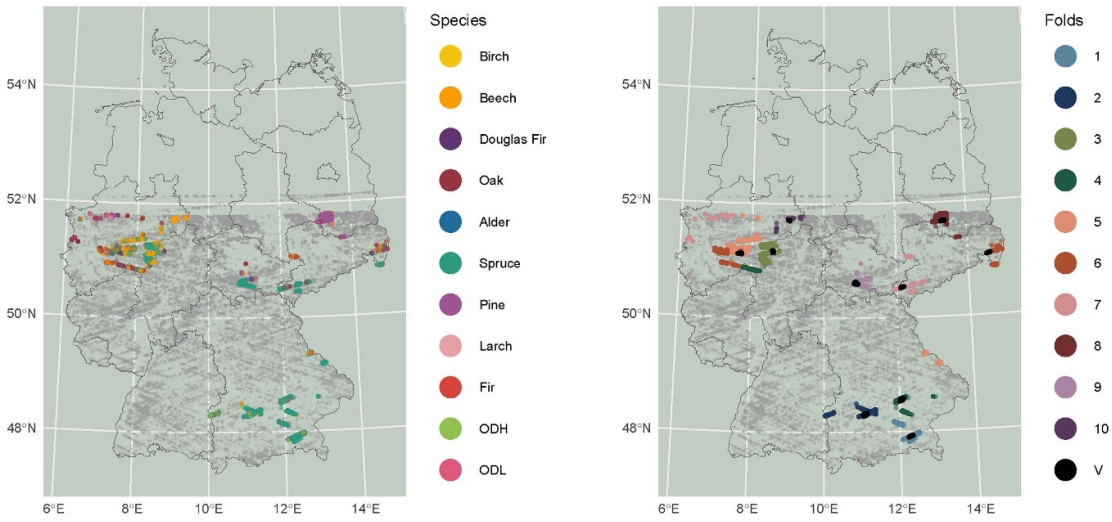

Figure 3. Maps displaying canopy fuels modeling data categorized by species (left) and cross-validation fold (right). Most common coniferous tree species (pine, spruce) are mainly spread throughout southern and eastern Germany, whereas common deciduous species (oak, beech) are predominantly found in western Germany. *k*-nearest neighbor distance matching (kNNDM) cross-validation folds each consist of one or more clusters. Validation samples (V) are represented by black dots. Background only shows a 5% random sample of GEDI observations used in this study (grey dots) to visualize overpass tracks.

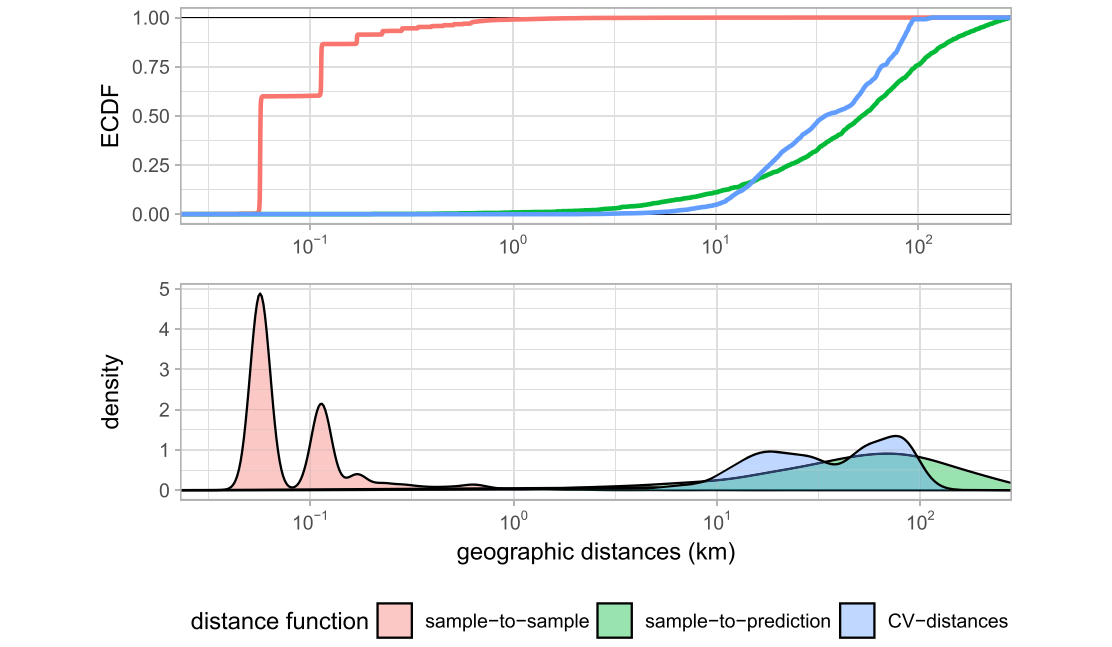

Figure 4. Density distribution (bottom) and empirical cumulative distribution functions (ECDF, top) of geographic nearest neighbor distances between sampling locations (red), sampling and prediction locations (green), and cross validation folds (blue). GEDI's along-track sampling distance of 60 m causes the larger peak in sample-to-sample distances. As a result of applying a *k*-nearest neighbor distance matching (kNNDM) spatial cross-validation, distances during model training and evaluation are matched to distances in model prediction.

similar distance distribution. We further sampled the modeling data with a 100 m grid (one random sample per grid cell) to reduce the effects of extreme clustering.

Footprint-level predictions were evaluated with a validation dataset ($n = 2405$) which was excluded prior to the model tuning process and also used later for the validation of final canopy fuel maps. The validation dataset was created by applying a 5 km buffer to one randomly selected sample per CV fold. All samples within this buffer were selected, adding up to approximately 20% of the training data.

We used Pearson correlation coefficient (R^2) to evaluate model fit and *RMSE* to quantify the mismatch between reference and model prediction. As absolute value ranges differ among target variables we added the

Table 2. Number of reference observations generated from airborne LiDAR at GEDI points (plots). The species label relates to individuals or to dominant species at plot-level. The uneven distribution among species results from spatio-temporal matching of both data sources, which revealed large overlaps in forested areas dominated by spruce, beech, and pine.

Species	Plots (%)	Individuals (%)
Birch	166 (2.0)	4221 (2.7)
Beech	1534 (18.0)	28 707 (18.7)
Douglas fir	260 (3.1)	6346 (4.1)
Oak	817 (9.6)	14 476 (9.4)
Alder	71 (0.8)	1232 (0.8)
Spruce	4286 (50.4)	70 784 (46.0)
Pine	990 (11.6)	20 055 (13.0)
Larch	270 (3.2)	4954 (3.2)
Fir	36 (0.4)	1292 (0.8)
ODH	53 (0.6)	1432 (0.9)
ODL	17 (0.2)	356 (0.2)
Total	**8500 (100)**	**153 855 (100)**

relative *RMSE* (*rRMSE*), calculated as *RMSE* divided by the standard deviation of the reference data, to compare models across target variables.

To assess our models' credibility throughout the study area we calculated the Area Of Applicability (AOA). Distances in the predictor space are computed between each prediction location and the Nearest Neighbor in the training dataset, resulting in the Dissimilarity Index (DI). A threshold is applied to distinguish whether prediction locations fall in- or outside the AOA (Meyer and Pebesma 2022). This applicability label indicates whether model performance metrics are reliable at a specific prediction location.

3.5.2. Map prediction

Raster maps were evaluated with the same validation set withheld in the previous modeling step. Additionally, raster maps were validated with independent canopy fuel estimates from publicly available NFI tree lists, produced via *FuelCalc*. Through cooperation with the administering institute (Thünen Institute for Rural Areas, Forestry and Fisheries), we received predicted canopy fuels at raster cell centers closest to each NFI plot center along with their corresponding identification code. This way, we could validate our model predictions while adhering to the NFI privacy regulations. The same performance metrics as for footprint-level estimates (R^2, *RMSE*) were applied to quantify the accuracy of the map prediction.

We investigated absolute and standardized model residuals using simple descriptive statistics. Residuals were obtained by subtracting model predictions from NFI-based validation estimates. Standardized residuals were computed by dividing residuals by the model prediction standard errors. We further evaluated remaining trends in the residuals using linear regression.

Finally, we create prediction error maps, which present the square root of the sum of the squared standard error from the linear model and the residual Kriging variance.

3.6. Software

This study was realized using the R programming language for statistical computing (R Core Team 2023) and its package ecosystem. Spatial data handling and processing was facilitated by *lidR* (Roussel *et al* 2020), *sf* and *stars* (Pebesma and Bivand 2023), *terra* (Hijmans *et al* 2022), *GLCMTextures* (Ilich 2020), and *rgee* (Aybar 2022) and supported by *dplyr* (Wickham *et al* 2023a), *tidyr* (Wickham *et al* 2023b), and *purrr* (Wickham and Henry 2023). Statistical modeling was carried out using *ranger* (Wright and Ziegler 2017), *caret* (Kuhn 2021), *CAST* (Meyer *et al* 2023), *gstat* (Pebesma 2004), and *automap* (Hiemstra *et al* 2008). Visualizations were designed with *ggplot2* (Wickham 2016), *ggpubr* (Kassambara 2023), *patchwork* (Pedersen 2022), and *basemaps* (Schwalb-Willmann 2022). Other software that supported this research includes the *spectral* library for GEE (Montero *et al* 2022) and *FuelCalc* (Reinhardt *et al* 2006).

4. Results

4.1. Footprint-level estimates based on airborne LiDAR data

The distribution of tree species at training locations is presented in table 2. It depended on environmental conditions found in areas where airborne and spaceborne LiDAR acquisitions overlap. Hence, the distribution may not be representative for the entire study area. Spruce, for instance, is over-represented (50.4%), while fir is under-represented (0.4%).

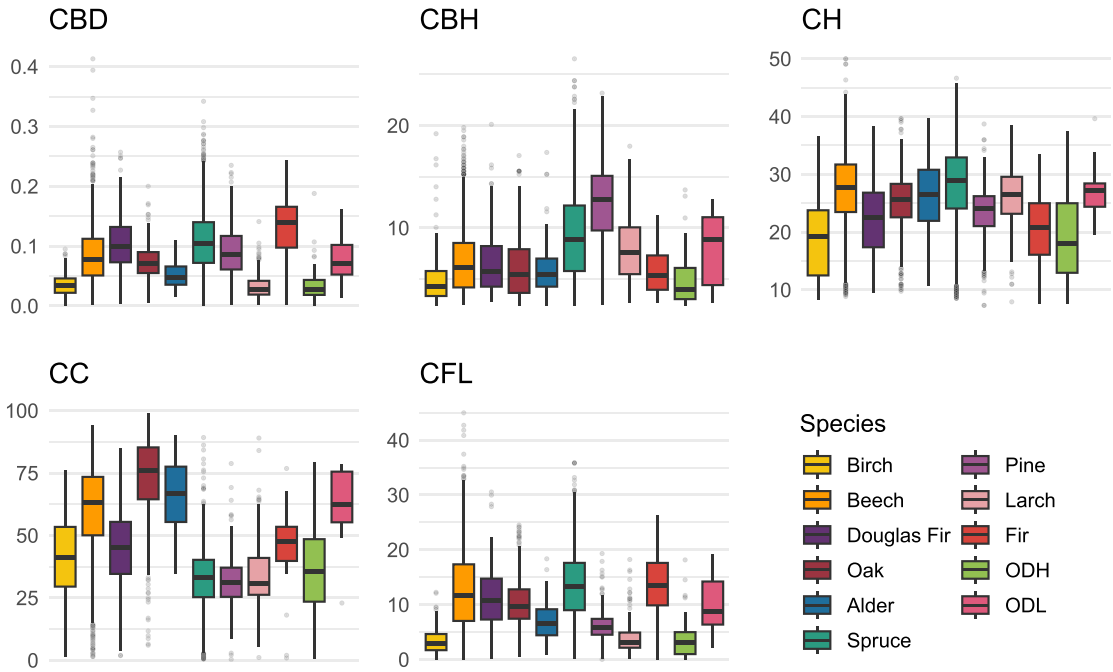

Figure 5. Footprint-level canopy fuel estimates derived from LiDAR-based tree-level structure metrics via species-specific allometric crown biomass equations. General differences in traits can be observed between broad-leaved and coniferous species. On average, broad-leaved species (e.g. beech and oak) tend to have higher canopy cover (CC) and lower canopy base height (CBH), whereas coniferous species (e.g. spruce and fir) have higher crown bulk density (CBD) and canopy fuel load (CFL). Differences are less distinctive for canopy height (CH).

Table 3. Performance metrics of Random Forest models predicting footprint-level (FP) canopy fuels based on GEDI measurements. Metrics are derived following model training with a *k*-nearest neighbor distance matching (kNNDM) spatial cross-validation (M) and through validation using a test dataset (V).

Model	*mtry*	*mns*	R^2_M	R^2_V	$RMSE_M$	$RMSE_V$	$rRMSE_M$	$rRMSE_V$
CBD_{FP}	13	5	0.55	0.48	0.03	0.03	0.68	0.73
CBH_{FP}	11	5	0.68	0.67	2.41	2.24	0.57	0.58
CH_{FP}	5	5	0.67	0.73	3.86	3.34	0.57	0.53
CC_{FP}	13	3	0.76	0.79	9.95	8.88	0.49	0.46
CFL_{FP}	11	7	0.63	0.59	4.03	3.91	0.61	0.64

Figure 5 shows value ranges and distributions of canopy fuel variables grouped by dominant species. Coniferous species feature higher medians for crown biomass variables crown bulk density (CBD) and canopy fuel load (CFL), whereas broad-leaved species develop higher canopy cover (CC) and lower canopy base height (CBH). CH does not reveal a strong species-dependence.

4.2. Footprint-level estimates based on GEDI data

We trained and evaluated RF models to predict five canopy fuel variables at footprint-level FP with GEDI measurements. Hyperparameter tuning yielded different structural complexity for each model. Optimal *mtry* was 13 for CBD_{FP} and CC_{FP}, 11 for CBH_{FP} and CFL_{FP}, and 5 for CH_{FP}. The best suitable *mns* was identified as 5 for CBD_{FP}, CBH_{FP} and CH_{FP}, 3 for CC_{FP}, and 7 for CFL_{FP}. Overall, performance metrics indicated satisfactory results. Table 3 presents a complete overview of final footprint-level model performance and hyperparameters, while scatter plots in figure 6 visualize the fit between validation data and model predictions based thereon. Due to the carefully chosen CV method, model metrics were expected to be more reliable than validation metrics in this first modeling step, as they stem from evaluating ten folds rather than from a single validation dataset. Validation metrics, however, were in close proximity to CV-derived metrics and did not suggest considerable bias.

CC_{FP} produced the best R^2 (0.76) and the lowest *rRMSE* (0.49). Its *RMSE* is reasonable at 9.95%. The corresponding validation scatter plot revealed a higher density in the low to medium value range (25%–50%) than for higher values. CBH_{FP}, CH_{FP} and CFL_{FP} scored acceptable R^2 between 0.63 and 0.68. Their prediction errors were larger than for CC_{FP} with *rRMSE* ranging from 0.57 to 0.61. CH_{FP} achieved fairly good validation scores and showed promising scatter plot densities for medium and tall canopies (>20 m), but suggests

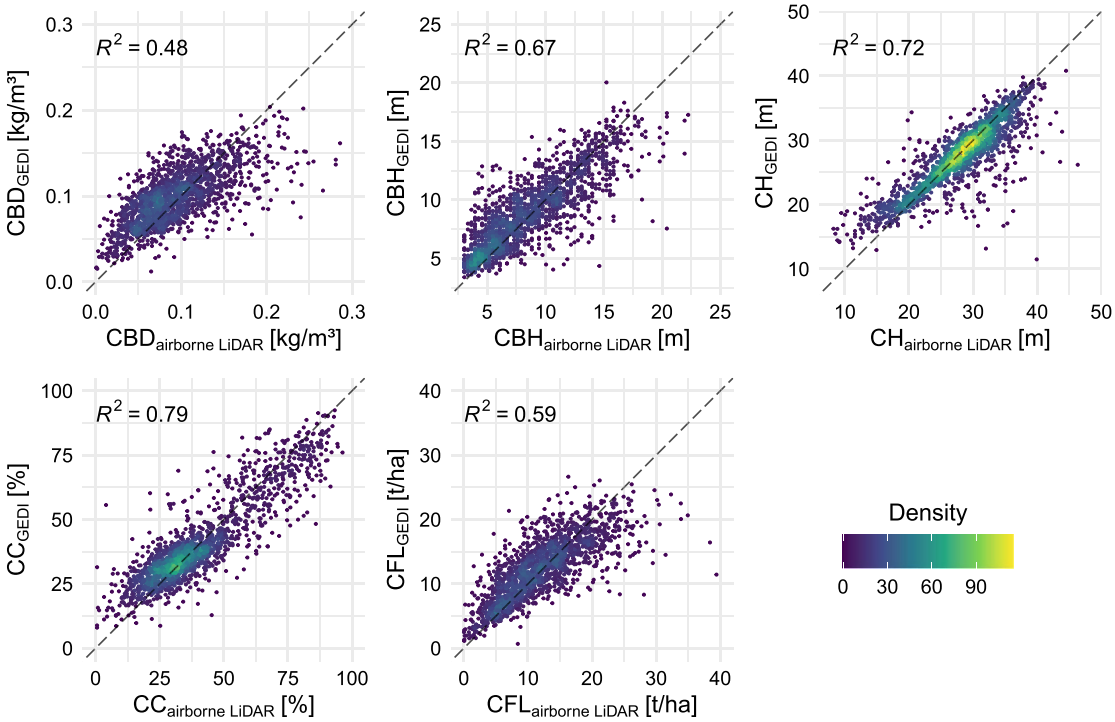

Figure 6. Agreement between footprint-level canopy fuel predictions and validation data compared to the identity line (dashed). *Y*-axis: Random Forest model predictions based on GEDI measurements and species information. *X*-axis: validation estimates based on segmented airborne LiDAR point clouds and allometric crown biomass equations.

overestimation of lower canopy heights. Least accurate among the five models was CBD_{FP} with an R^2 of 0.55 and an *rRMSE* of 0.68. Validation plots of CBD_{FP} and CFL_{FP} show moderate signs of heteroscedasticity.

In figure 7 we display the 15 most important predictor variables per model to compare their individual contribution. An additional graph is dedicated to the across-model average. Some footprint-level predictors are strongly correlated (e.g. relative height metrics in five percent increments). Appendix figure A1 presents the respective correlation matrix. Variable importance scores of single variables should, hence, be treated carefully, while it is more sensible to consider groups of similar predictors. Tree species was the most relevant predictor for CC_{FP}, for CFL_{FP}, and overall, followed by the upper relative height metrics. Foliage height diversity (*fhd_normal*) was listed among the top predictors of all models. The largest contribution to the accuracy of CC_{FP} came from dominant species labels and variables describing footprint-level species composition, especially fractions of the most abundant broad-leaved species oak and beech. Unexpectedly, GEDI's cover metrics were not very relevant for the model. Upper relative height metrics were the most powerful predictors for CH_{FP} and CBH_{FP}. Species information considerably supported CBH_{FP}, but was not relevant for CH_{FP}. As species differ more in branch and canopy structure than in height, this is comprehensible from an ecological standpoint. Next to species, CFL_{FP} depended on AGBD, upper relative heights, and portions of coniferous species (spruce, pine, and larch). AGBD appears to be a logical choice to predict CFL because both variables characterize biomass. Same applies to tree height as it correlates with biomass. Further, coniferous trees tend to have higher bulk densities (see figure 5), which drives footprint-level CFL and CBD. Other influential predictors for CBD_{FP} were relative heights in the third quartile, which are typically the heights where the largest tree-level CBD values can be observed.

The AOAs of the five models appear very similar because they all rely on the same training dataset. Differences stem from individual variable importance weights. Figure 8(top row) shows the density distributions of the DI for training versus prediction locations. Both curves mostly overlap, indicating large agreement of distances in the predictor space and, hence, applicability of the models to the largest part of prediction locations. Overall, the percentage of prediction footprints outside the AOA were low (CBD_{FP}: 2.5%; CBH_{FP}: 4.4%; CH_{FP}: 4.7%; CC_{FP}: 4.0%; CFL_{FP}: 3.6%). In a spatial context, the AOA identified regions in which increased portions of GEDI prediction locations fell beyond the DI threshold. Raster maps in figure 8 present the ratio of footprints inside the AOA aggregated to 5 km raster cells. Most noteworthy is the central Black Forest region in the south-west of Germany, where the ratio of footprints inside the AOA drops below 50%. This may be explained by the dominance of fir trees in the area, which are strongly underrepresented in the reference data (see table 2). The occurrence of fir is concentrated in this part of the

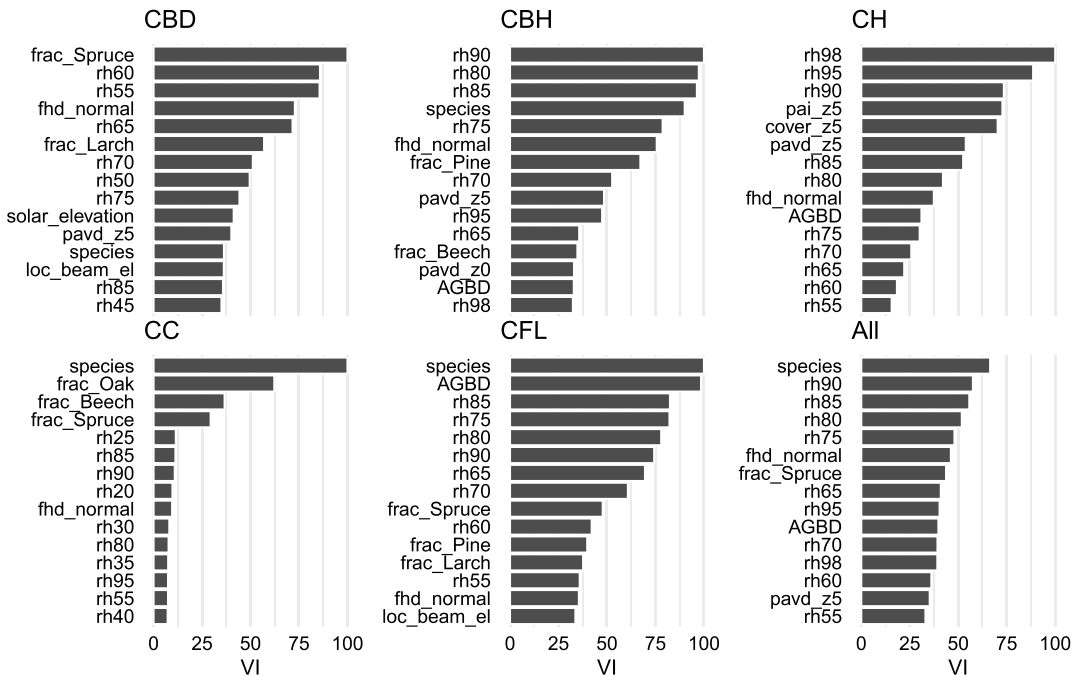

Figure 7. Variable importance scores for final footprint-level canopy fuel Random Forest (RF) models. Species and species composition played a crucial role in predicting all canopy fuel variables, except for canopy height (CH_{FP}). Relative heights, especially in the upper percentiles, were GEDI's most relevant predictors.

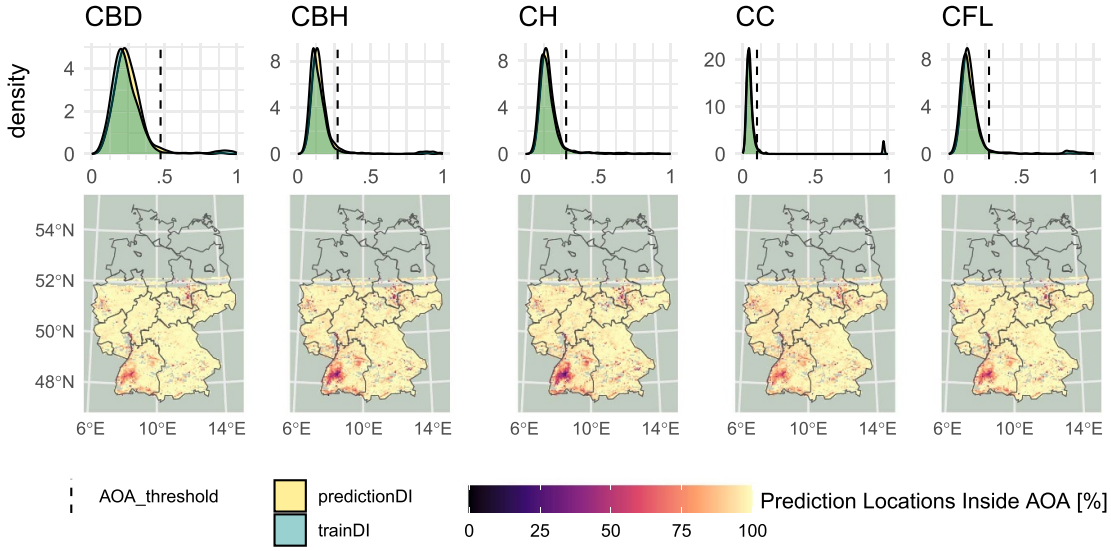

Figure 8. Top row: density distribution of the Dissimilarity Index (DI) for training (blue) and prediction (yellow) locations. Curves mostly overlap (green) which implies substantial similarity of distances in the predictor space of training and prediction sets of footprint-level models. Locations beyond the threshold (dashed line) fall outside of the Area of Applicability (AOA). Bottom row: spatial distribution of prediction locations inside the AOA aggregated to 5 km raster cells. Locations fall within the threshold for most parts of the study area, except for few small cases and the central Black Forest in the south-west. This region is dominated by fir, which is underrepresented in the reference data.

study area, and airborne LiDAR data are not available in the state of Baden-Württemberg. Therefore, models were not trained for such conditions, making them less applicable here. Same applies to areas at the southern country border where higher elevations drive species composition and canopy structure.

4.3. Map prediction

Table 4 compares performance metrics of the individual map prediction steps: model, model prediction, and universal Kriging prediction. Except for CC, model and validation R^2 dropped considerably when benchmarked with their footprint-level counterparts, whereas model *RMSE* values were almost equal

Table 4. Performance metrics for all three components of the canopy fuels map prediction: linear regression models (*LM*), their validation with data excluded previous to model training (V_{LM}; $n = 1692$) and validation of the final universal Kriging output (V_{UK}), i.e. sum of linear model prediction and residual Kriging. Validation metrics were generally poorer than model metrics. Universal Kriging achieved higher accuracy for all variables compared to linear models alone.

	R^2			*RMSE*			*rRMSE*		
Model	*LM*	V_{LM}	V_{UK}	*LM*	V_{LM}	V_{UK}	*LM*	V_{LM}	V_{UK}
CBD_{Map}	0.34	0.21	0.24	0.02	0.04	0.04	0.81	1.97	1.96
CBH_{Map}	0.36	0.25	0.35	2.32	3.38	3.19	0.80	2.17	1.92
CH_{Map}	0.31	0.35	0.42	4.01	5.21	4.99	0.83	1.82	1.55
CC_{Map}	0.78	0.64	0.65	8.58	11.86	11.66	0.47	0.86	0.78
CFL_{Map}	0.45	0.34	0.36	3.67	4.99	4.88	0.74	1.61	1.50

Table 5. Performance metrics describing the validation with independent canopy fuels estimates based on National Forest Inventory (NFI) tree lists. The same metrics from table 4 are calculated for spatial predictions at NFI plot locations ($n = 50\,351$). Model residuals are characterized in more detail by their mean $\bar{X}$ and standard deviation σ. Further, R^2 describes multiple linear regression of residuals using all 92 predictors and expresses potential improvement in case NFI data was available for modeling. *RMSE* and σ provide insight into the distribution of standardized residuals (residuals divided by the prediction standard error).

		residuals					*st.residuals*	
Model	R^2	*RMSE*	*rRMSE*	$\bar{X}$	σ	R^2	*RMSE*	σ
CBD_{Map}	0.06	0.09	4.38	0.02	0.09	0.27	3.89	3.76
CBH_{Map}	0.11	3.96	1.98	0.77	3.88	0.10	1.71	1.68
CH_{Map}	0.25	6.30	1.85	0.58	6.28	0.07	1.70	1.70
CC_{Map}	0.09	21.82	1.38	4.36	21.37	0.19	2.61	2.56
CFL_{Map}	0.09	7.07	1.85	−5.71	4.17	0.47	2.12	1.27

(compare table 3). Residual Kriging improved the accuracy of all map predictions. Largest gains were observed for CBH (R^2: +0.1; *RMSE*: −0.19) and CH (R^2: +0.07; *RMSE*: −0.22).

Table 5 shows validation results for an independent set of canopy fuels estimates based on NFI data ($n = 50\,351$). Modest to low R^2 values indicate that the variability in both sets of estimates is weakly related. *RMSE* and *rRMSE* values are substantially higher than those of the validation using withheld data shown in table 4. A comparison of validation metrics for predictions within versus outside of GEDI's spatial domain did not yield notable differences.

We also computed statistics for standardized residuals, where residuals (observed—predicted) are divided by the standard error of the predicted values. Ideally, standardized residuals have an *RMSE* of one. In case it is larger than one (as in our case), this can be caused by bias in the predictions, by an underestimation of the prediction standard error, but also by bias or variance in observed values. Since we have no information about the bias or variance of the observed NFI values, it is difficult to draw hard conclusions based on our comparison.

All variables have an *RMSE* of standardized residuals larger than one, but in different degrees: the height-related models (CBH_{Map}, CH_{Map}) are closer to one than the others. Overall, this means that there is a bias in our model predictions, or an underestimation of our model prediction standard errors, or a bias and/or variance in the validation data, or a combination of those. Figure 9 shows histograms of standardized residuals, and clearly indicates which models are biased in this comparison (some bias for CC_{Map}, strong bias for CFL_{Map}).

The R^2 values of the residuals sub-table of table 5 reflect those of a multiple linear regression model where residuals are regressed on all the 92 predictors. These values indicate how much the regression components of our map predictions *could* have been improved, had the NFI values been available with precise geographic coordinates. For CFL_{Map} a considerable improvement could have been obtained, for CH_{Map} and CBH_{Map} this improvement potential is modest.

Figure 10 shows two example locations with universal Kriging results, while appendix figure A2 shows corresponding maps for Germany. One is situated in Brandenburg, east Germany (red marker), where pine is widely spread with oak stands scattered in between. CBH, CC, and CFL demonstrate a strong species-dependence, as pine has a higher canopy base, lower cover due to sparser crowns, and lower overall fuel load. Higher CBD values coincide with higher CH, especially in pure pine stands. A second location is based in southern Bavaria (blue marker) where the forest is dominated by spruce, sporadically mixed with beech and other species. Species-related patterns in CBH, CC, and CFL are visible, yet less distinct. Spruce trees are taller and have lower canopy bases, which leads to tall crowns with more canopy layers and biomass compared to pine trees. Maps of CBD and CFL demonstrate this relationship, as the highest values are found

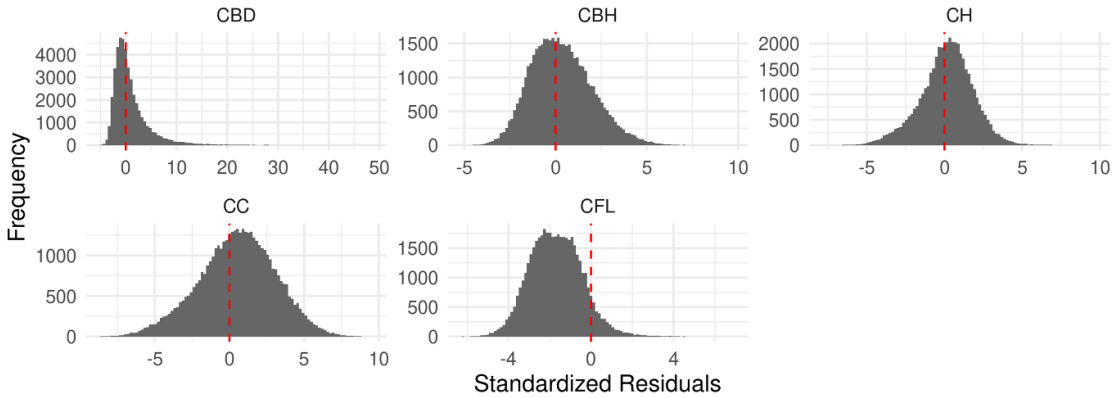

Figure 9. Histograms of standardized residuals between canopy fuel predictions and validation estimates based on National Forest Inventory (NFI). Red dashed line marks $x = 0$. Height-related variables show weak bias, while crown bulk density (CBD_{Map}), canopy cover (CC_{Map}), and especially canopy fuel load (CFL_{Map}) show stronger bias.

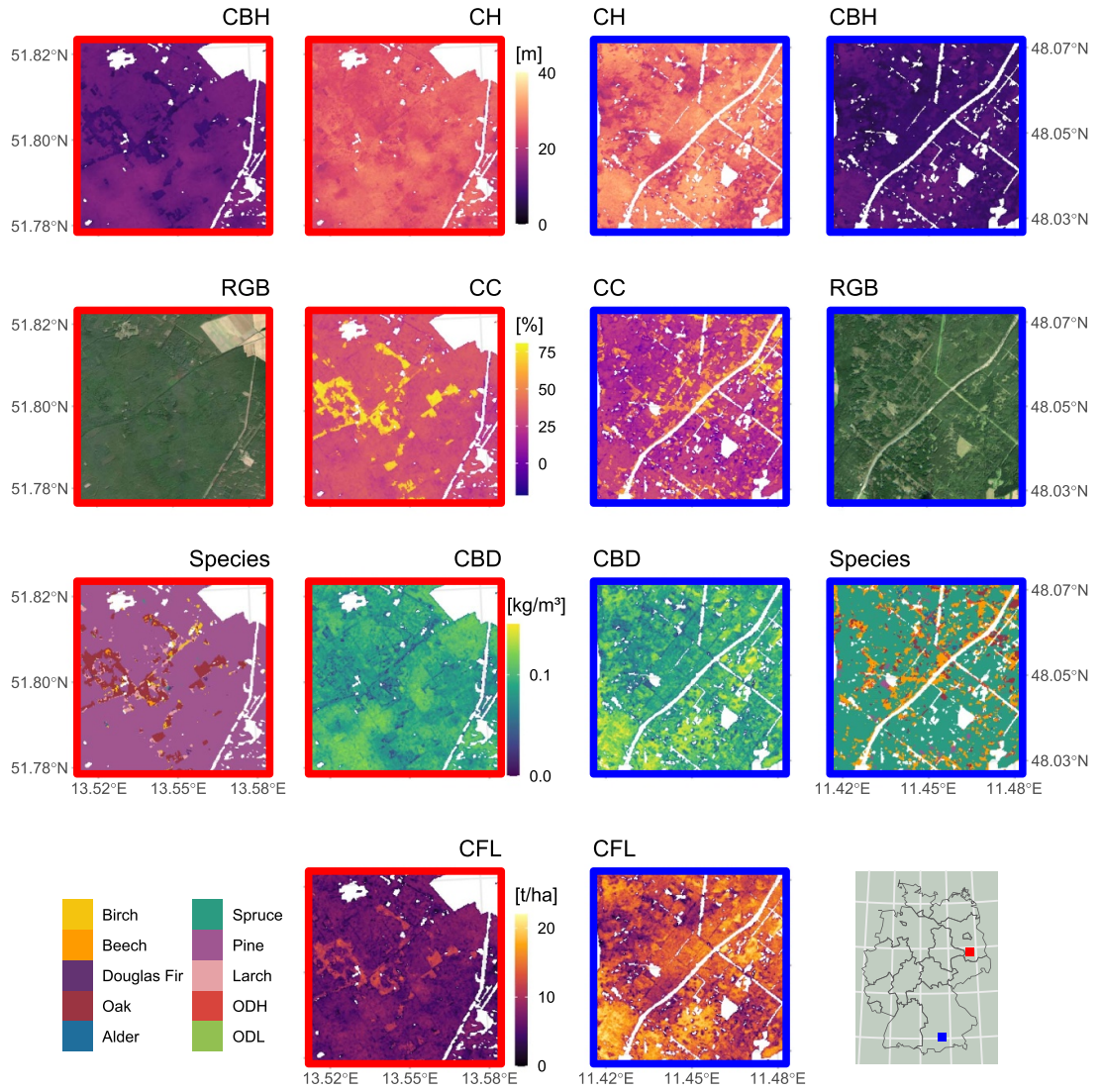

Figure 10. Two example locations (5 × 5 km) showing canopy fuel prediction results. Canopy base height (CBH) and canopy height (CH) share the same scale. Located in Brandenburg, eastern Germany (red marker and map frames), pine shows higher crown bulk density (CBD) than oak, but lower canopy cover (CC) and canopy fuel load (CFL). A spruce-dominated forest in southern Bavaria (blue marker and map frames) is estimated to develop higher CH, CC, CBD, and CFL, thereby producing more burnable biomass. RGB imagery was accessed through Mapbox.

in pure spruce stands. The spruce-dominated forest provides considerably more canopy fuels than pine forests.

Appendix figure A3 displays prediction error maps for each canopy fuel variable, respectively. All maps clearly indicate an abrupt increase in prediction errors north of the GEDI data acquisition range (51.6° N). This also applies to areas, e.g. in south-western or central-eastern parts of Germany, where GEDI orbits and therefore footprint-level estimates for residual Kriging are spaced further apart. In areas with a sufficient density of GEDI footprints, prediction errors were lower (CH: 3–4 m; CBH: ∼2.3 m; CC: 8%–9%; CBD: 0.024–0.026 kg m^{-3}; CFL: 3–3.6 t ha^{-1}). Areas beyond GEDI's acquisition range show substantially greater prediction errors (CH: 4–4.5 m; CBH: ∼2.4; CC: 9%–9.5%; CBD: 0.026–0.027 kg m^{-3}; CFL: 4–4.3 t ha^{-1}). In all cases, the largest proportion of the error stems from the residual Kriging variance, while the squared standard error of the linear model contributed only a small percentage.

5. Discussion

We proposed an elaborate two-step methodology that predicts canopy fuels firstly at footprint-level, and then, from those predictions, predicts country-wide raster maps. A more straight-forward approach would avoid GEDI data and simply feed footprint-level estimates and covariates to a ML model directly. GEDI, however, may currently be the most advanced spaceborne sensor for measuring vertical vegetation structure at the near-global scale. For this reason we had higher expectations for GEDI measurements to accurately predict canopy fuels than for common two-dimensional covariates. To provide useful resources for fire spread simulations and related risk and hazard assessments we had to select a spatial prediction technique. GEDI footprints are abundant and cover large parts of the study area, which are attributes that enable geostatistical methods. We opted for universal Kriging following the assumption, that spatial variability of canopy fuels was not random, but (partially) depended on biophysical covariates. Linear regression models and Kriging are both simple and therefore transparent statistical methods suitable for spatial prediction.

An advantage of our approach is that third parties can use our pre-trained RF models to predict canopy fuels from future GEDI measurements, provided that species information is available. Despite only producing footprint-level estimates, this may be sufficient for expert users, e.g. forest management, who can transfer insights to fulfill their objectives without needing raster maps. They may alternatively choose their own spatial prediction or aggregation method while applying different or updated covariates. As footprint-level models are more reliable, this procedure is recommended for users investigating small areas or new domains. Our five country-wide map products have the benefit of originating from the same data and methodology. That assures consistency among canopy fuel variables and has positive implications for subsequent fire modeling. As a drawback of the two-step approach, errors from the first model predictions are propagated to the reference data in the second step. This contributes to the drop in accuracy observed in table 4 (compared to table 3).

Footprint-level models should be transferable to regions with species similar to the set of proxy species considered for calculating crown biomass. Especially the vertical distribution of crown biomass and densities of particle size classes should match. Yet, models are expected to be most reliable inside homogeneous forests. Forest edges with their variable biophysical conditions were excluded when generating the reference data. Hence, models may produce erroneous predictions in these areas.

We transferred the footprint-level models beyond GEDI's acquisition range (51.6° N) to include northern Germany in the predicted canopy fuel maps. While there is a similarity in tree species composition and silvicultural practice between the two regions north and south of 51.6° N, we acknowledge a certain degree of geographic and climatic variation. Hence, model training and model prediction are carried out with data from regions with different bio-climatic conditions. Predictions in northern Germany should therefore be considered as an extrapolation of the model to a new domain. Prediction error maps provided along with the final maps allow downstream users to assess the quality of the prediction (see appendix figure A3). For each canopy fuel variable, these maps clearly indicate a considerable jump in error values for locations lacking GEDI data. Future efforts could address this caveat by supplementing GEDI with other spaceborne LiDAR measurements that cover this region, e.g. from the ICESat-2 mission.

Because allometric equations are species-specific, the species label is a crucial predictor in our models. For instance, the four most important predictors for CC_{FP} consisted of tree species and species composition, not more obvious GEDI measurement variables describing canopy structure. This indicates a discrepancy between estimates from empirical, allometric models designed for fire behavior assessment and space-borne measurements. The species-dependency exposes additional challenges since labels are extracted from a 10 m classification raster, which stores a single dominant species per cell. Synthetic tree lists may hence not capture the actual footprint-level species diversity, which is a more profound problem in mixed forests. When transferring our method to another large region, obtaining accurate (satellite-based) tree species information

may be difficult. For small areas, however, high-resolution stand maps from, e.g. forestry administrations could improve the models and lead to better results.

Even though GEDI's geolocation error has been improved in version 2 it is still considerably high (10.3 m) compared to its measurement footprint (25 m). An attempt to correct footprint locations using *rh98* and CH from airborne LiDAR was not successful. This, however, does not mean that footprint locations cannot further be improved, but rather that CH in close proximity to the original locations gave no reason to adjust them. Yet, the location error can still have a considerable impact on other canopy fuel variables. Except for CC, these cannot be derived from point clouds directly and could therefore not be included in the location correction. Displaced footprint centers lead to different point cloud subsets and cause the detection of different individuals or the assignment of wrong species labels. Thus erroneous synthetic tree lists result in inaccurate footprint-level canopy fuel estimates which form the training data for predictive models. The magnitude of this effect, however, depends on forest stand heterogeneity, which we assume to be limited as the majority of forests in Germany are managed using conventional silviculture.

Synthetic tree lists may further be affected by algorithm selection and parameters in the segmentation process. These should be chosen based on stand properties like age, structure or silvicultural strategy (Li *et al* 2012). Homogeneous beech stands for example may require different parameters than heterogeneous mixed forests. Highly individual parameter selection could not be realized in this analysis step. The number of individuals per footprint and hence footprint-level canopy fuel estimates may have been underestimated.

Raster covariates used for spatial prediction each come with errors. Especially derived remote sensing products such as biomass, leaf traits, or phenology carry uncertainty from previous modeling efforts. Resampling and reprojection may have introduced further inaccuracy. Note that increasing the spatial resolution of some products through resampling did not add new information.

The validation with NFI-based estimates revealed some interesting differences between the canopy fuel values produced with the two distinct methods. CBD shows a strong disagreement, CH and CBH show a relatively strong agreement, and CFL shows a bias but otherwise relatively good agreement given the prediction errors of our procedure. It should be noted here that the NFI forest structure measurements comprise a completely independent source of data, and their canopy fuel variables are the result of estimation as well. On the other hand, the dominant tree species map by Blickensdörfer *et al* (2022) is derived from NFI species labels. Our RF models identified this dataset as one of the most important covariates for their canopy fuel predictions. Therefore, our validation might be positively biased towards the NFI data.

Generating species-level remote-sensing datasets is important for applying our methodology in other areas, but still remains a challenge (Fassnacht *et al* 2024). Current research addresses this gap by developing different models for high-resolution tree species mapping (Schiefer *et al* 2020, Bonannella *et al* 2022, Hermosilla *et al* 2022).

The errors of the NFI-based canopy fuel estimates are unknown, and, if non-zero, do contribute to the differences we observe in this validation to a degree that we cannot determine. More in detail, error components in this comparison beyond the prediction errors of our predicted values may be attributed to the following factors:

- The allometric crown biomass equations used for the NFI estimates make simplifying assumptions to summarize tree lists into single footprint-level values.
- Besides GEDI's location error, NFI plot center coordinates are subject to GPS inaccuracy, which affects, e.g. matching the corresponding pixel center during the validation of raster map values.
- The NFI plots were recorded using a flexible radius (Bitterlich method), which leads to estimates associated with a surface area different from the 20 m pixels of our predictions, and hence a mismatch in spatial *support*.
- The NFI plot data were collected in 2012, temporal forest dynamics may contribute to the differences observed in this comparison.

Nevertheless, with *RMSEs* of 6.3 m for CH_{Map} and 21.8% for CC_{Map}, the accuracy of our model predictions is in line with other large-scale spatial prediction studies that use GEDI and multi-spectral satellite data. CH maps by Potapov *et al* (2021), which are predicted using Landsat data, come with *RMSEs* of 6.6 m when evaluated against withheld GEDI observations and 9.1 m when validated with airborne LiDAR. Lang *et al* (2022) achieved slightly better *RMSEs* with their Deep Learning approach and Sentinel-2 data (5.2 m for GEDI observations and 7.8 m for airborne LiDAR). Kacic *et al* (2023) report an *RMSE* of 6.6 m for CH and 19.1% for CC after validating with a set of withheld GEDI observations. R^2 of our footprint-level predictions are comparable, whereas for our map predictions they are one order of magnitude lower than those of Kacic *et al* (2023), which can be expected, because the NFI-based validation data we used is a different source than our training inputs. For CBH_{Map}, CFL_{Map}, and CBD_{Map}, our predictions are currently the only data products of their kind covering Germany, which is why their accuracy is not discussed here as for CH_{Map} and CC_{Map}.

Prediction error maps provided along with our map products aid users in making informed decisions when utilizing our canopy fuel maps.

6. Conclusion

Our study demonstrates a workflow to map canopy fuels at country level purely based on openly accessible data. It combines the advantages of various remote sensing techniques to gain insight into the three-dimensional structure of forests. Although conceding errors and uncertainties, our method enables the generation of large-scale canopy fuel maps without requiring extensive field measurements and manpower. We assure reliability of footprint-level outputs by applying a suitable spatial CV and by assessing model applicability. Map validation with NFI-based estimates reveals low to modest agreement. A subsequent error analysis supports the assumption, that predicting canopy fuel variables with two-dimensional data is challenging. It further suggests, that better results could be obtained if NFI data were fully open. Canopy fuel maps produced for Germany can support wildfire risk and hazard assessments at local, regional, and national level. Example downstream applications of this data include scenario-based fire spread modeling or fuels management informed by fire behavior calculations. This workflow may serve as an example for regions where fire has rapidly emerged to a new threat and where expertise and information are still being established.

Data availability statement

Canopy fuel maps produced in this study can be explored in a GEE app at https://ee-forestfuels-ger.projects.earthengine.app/view/gedi-fuels. Analysis code and a demo subset of the data are available at https://github.com/joheisig/CanopyFuels_demo.

The data that support the findings of this study are openly available at the following URL/DOI: https://zenodo.org/doi/10.5281/zenodo.8285 855 (Heisig *et al* 2025).

Acknowledgements

We would like to thank Duncan Lutes from the Missoula Fire Science Laboratory for valuable comments on crown biomass models and the use of *FuelCalc*. Further, we thank Dr Sebastian Schnell from the Thünen Institute of Forest Ecosystems for support with the NFI-based validation of our final map products. Calculations (or parts of them) for this publication were performed on the HPC cluster PALMA II of the University of Münster, subsidised by the DFG (INST 211/667-1).

Author contributions

Johannes Heisig: Conceptualization, methodology, software, data curation, formal analysis, validation, visualization, writing—original draft, writing—review and editing, project administration. Milutin Milenković: Conceptualization, writing—review and editing. Edzer Pebesma: Conceptualization, methodology, resources, supervision, writing—review and editing.

Appendix

Table A1. GEDI Level 2A/B metrics and other supplementary variables used in predicting canopy fuels at footprint-level.

Level	Variable	Description	N
2A	rh_z	Relative height metrics at 5% intervals from 5 to 95 (plus percentile 98)	20
2B	cover	Total canopy cover	1
	cover_z	Cumulative canopy cover vertical profile at heights 0, 5, and 10 m	3
	fhd_normal	Foliage Height Diversity	1
	local_beam_azimuth	Azimuth of the unit pointing vector for the laser	1
	local_beam_elevation	Elevation of the unit pointing vector for the laser	1
	pai	Total Plant Area Index	1
	pai_z	Plant Area Index profile at heights 0, 5, and 10 m	3
	pavd	Total Plant Area Volume Density	1
	pavd_z	Plant Area Volume Density profile at heights 0, 5, and 10 m	3
	pgap_theta	Total Gap Probability	1
2A/B	sensitivity	Maximum canopy cover that can be penetrated	1
	solar_azimuth	Solar Azimuth	1
	solar_elevation	Solar Elevation	1
other	species	extracted from Blickensdörfer *et al* (2022)	1
	frac_species	Plot-level fractions of area covered by each species	11
	AGBD	Above-ground biomass density as calculated in Duncanson (2022)	1
	GFC_lossyear	Year of tree loss reported by Hansen *et al* (2013)	1
	year	Year of acquisition	1
	doy	Day of year	1
			55

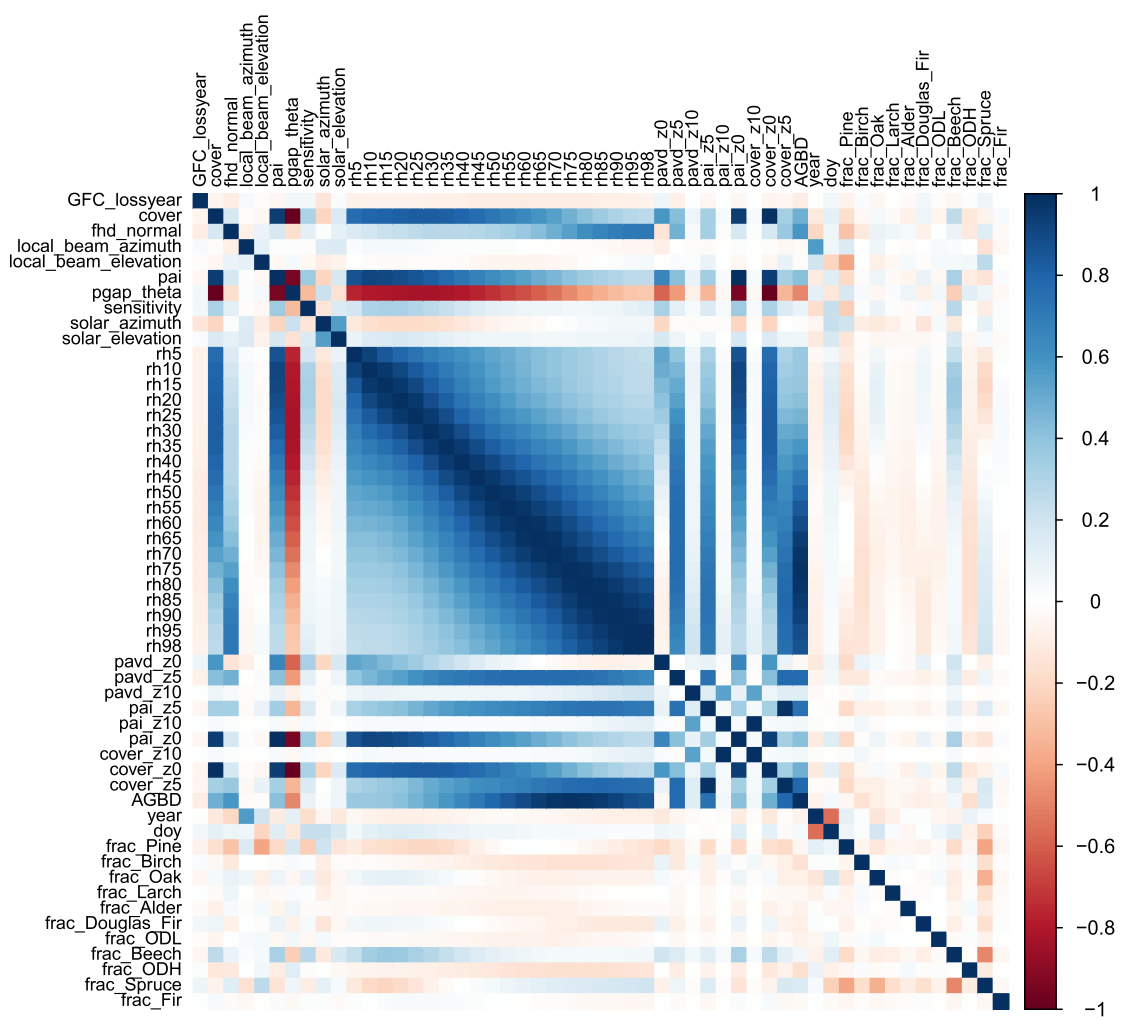

Figure A1. Correlation matrix of footprint-level predictors from GEDI Level 2A/B and other source (see appendix table A1 for details). Species label is a categorical variable and can, therefore, not be correlated to numeric variables.

Table A2. Covariate datasets for the reference year 2018 used in the map prediction step. Eight source datasets were disaggregated to individual variables, e.g. bands and reduced in the temporal or spectral dimension where appropriate, resulting in 92 individual raster covariates.

Dataset	Variable(s)	Res. (m)	Source
EU-DEM v1.1	Elevation Slope, Aspect	25	EU, CLMS, EEA (2023) derived
Dominant Tree Species	Species	10	Blickensdörfer *et al* (2022)
Sentinel-1 backscatter	VV, VH VV/VH ratio VV/VH-GLCM (contrast, dissimilarity, homogeneity, variance, correlation, ASM, mean, entropy)	25	ESA (2023) derived derived
Sentinel-2 surface reflectance	Bands 1-8, 8A, 11, 12 NDVI, NDWI, EVI, EVI2, SAVI	10	ESA (2023) derived
Sentinel-2 Vegetation Phenology Parameters	Productivity, PPI (min., max.), Growing Season (Start, End, Length)	10	EU, CLMS, EEA (2023)
PalSAR-2 backscatter v2	HH, HV HH/HV ratio	25	Shimada *et al* (2014) derived
MODIS Leaf Traits	SLA, LDMC, LNC, LPC, LNPR	500	Moreno-Martínez *et al* (2018)
CCI Biomass v3	Biomass	100	Santoro and Cartus (2021)

Table A3. Local tree species and their North American proxy species for allometric crown biomass calculation. Plot-level canopy fuels estimates rely on the assessment of individual crown components categorized by diameter. Component group (CG) 1 includes total crown, foliage, and twig (<0.6 cm) biomass. CG 2 describes branch biomass in three size classes (0.6–2.5 cm, 2.5–7.5 cm, >7.5 cm). Equations for twelve proxy species were used to describe crown components: Bigleaf Maple (BM), Douglas Fir (DF), Engelmann Spruce (ES), Grand Fir (GF), Giant Chinkapin Oak (GC), Lodgepole Pine (LP), Northern Red Oak (RO), Quaking Aspen (QA), Red Alder (RA), Tan Oak (TO), Western Larch (WL), Yellow Birch (YB).

	Proxy		Equation reference	
Local	CG 1	CG 2	CG 1	CG 2
Birch	YB	RA	Snell and Little (1983)	
Beech	TO	RA	Snell and Little (1983)	
Doug. Fir	DF		Brown (1978)	
Oak	RO	GC	Loomis and Roussopoulos (1978)	Snell and Little (1983)
Alder	RA		Snell and Little (1983)	
Spruce	ES		Brown (1978)	
Pine	LP		Brown (1978)	
Larch	WL		Brown (1978)	
Fir	GF		Brown (1978)	
ODH	QA	BM	Loomis and Roussopoulos (1978)	Snell and Little (1983)
ODL	QA	BM	Loomis and Roussopoulos (1978)	Snell and Little (1983)

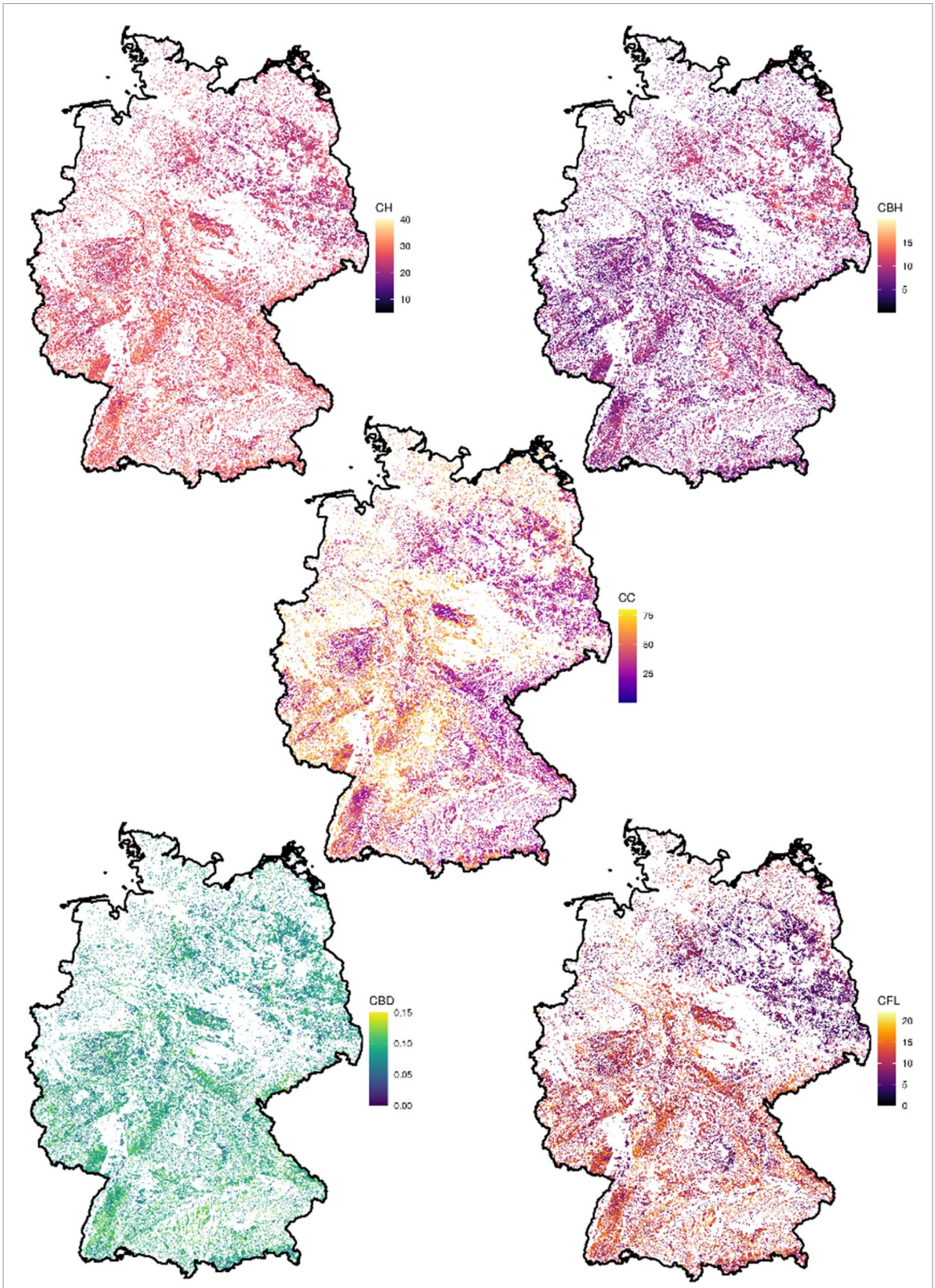

Figure A2. Countrywide map predictions of canopy fuel variables at 20 m spatial resolution: Canopy height (CH), canopy base height (CBH), canopy cover (CC), crown bulk density (CBD), and canopy fuel load (CFL).

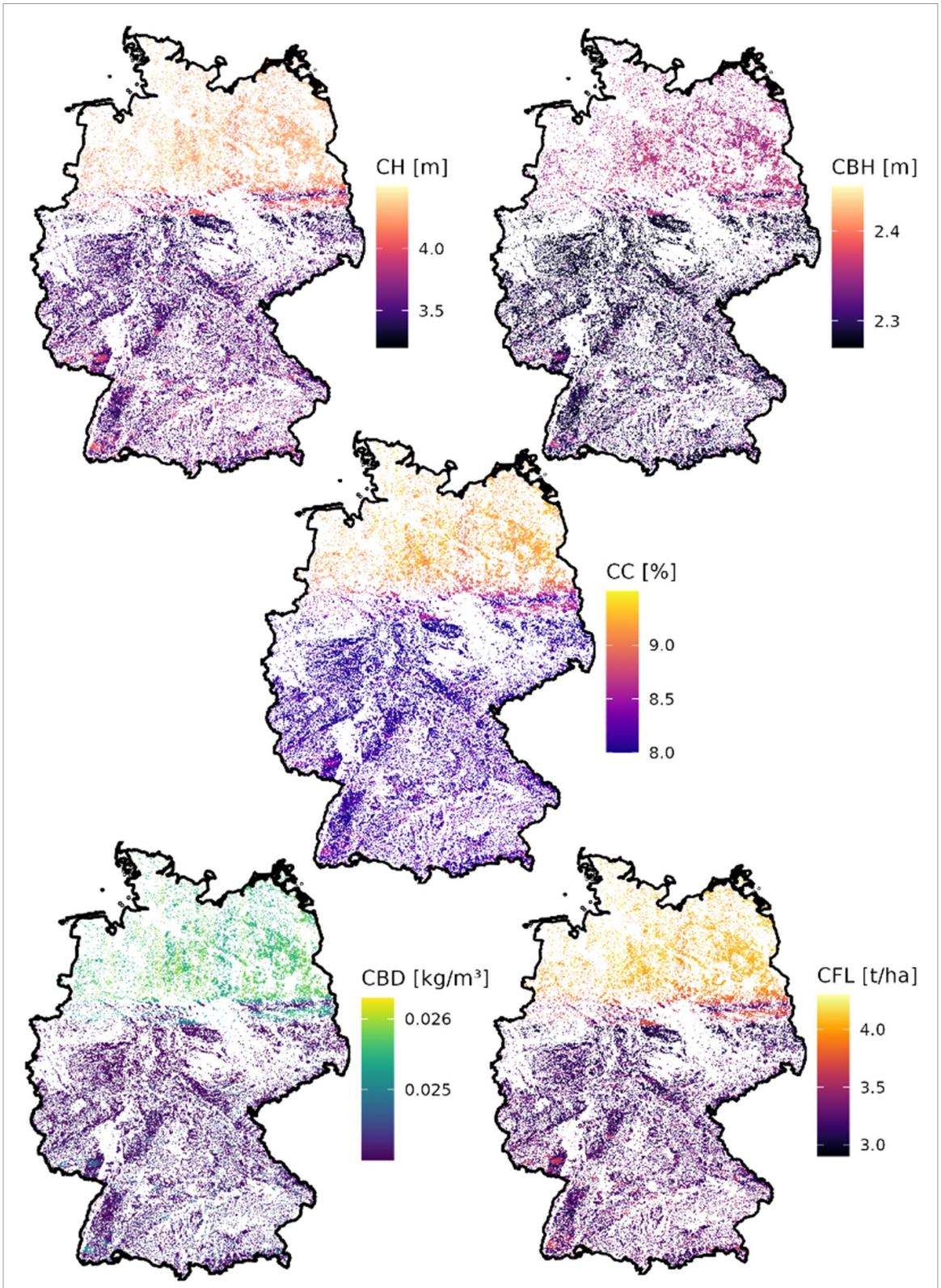

Figure A3. Countrywide maps of canopy fuel prediction errors at 20 m spatial resolution: Canopy height (CH), canopy base height (CBH), canopy cover (CC), crown bulk density (CBD), and canopy fuel load (CFL). Prediction error is defined as the square root of the sum of squared standard errors of the linear model and Kriging variance.

ORCID iDs

Johannes Heisig https://orcid.org/0000-0003-3586-3001
Milutin Milenković https://orcid.org/0000-0003-3256-6669

References

Andersen H-E, McGaughey R J and Reutebuch S E 2005 Estimating forest canopy fuel parameters using LIDAR data *Remote Sens. Environ.* **9** 13
Arroyo L A, Pascual C and Manzanera J A 2008 Fire models and methods to map fuel types: the role of remote sensing *Forest Ecol. Manage.* **256** 1239–52
Aybar C 2022 RGEE: R Bindings for calling the 'Earth Engine' *API* (available at: https://CRAN.R-project.org/package = rgee)
Baddeley A, Rubak E and Turner R 2016 *Spatial Point Patterns: Methodology and Applications With R* (*CRC Interdisciplinary Statistics Series*) (Champan & Hall, CRC Press, Taylor & Francis Group)
Beck J, Wirt B, Armston J, Hofton M, Luthcke S and Tang H 2021 Global ecosystem dynamics investigation (GEDI) level 2 user guide *Technical Report* The USGS Earth Resources Observation and Science (EROS) Center: NASA's Land Processes Distributed Active Archive Center (LP DAAC)
Berninger A, Lohberger S, Stängel M and Siegert F 2018 SAR-based estimation of above-ground biomass and its changes in tropical forests of Kalimantan using L- and C-band *Remote Sens.* **10** 831
Bivand R S, Pebesma E J and Gómez-Rubio V 2008 *Applied Spatial Data Analysis With R* (Springer)
Blickensdörfer L, Oehmichen K, Pflugmacher D, Kleinschmit B and Hostert P 2022 *Dominant Tree Species for Germany (2017/2018)* (Johann Heinrich von Thünen-Institut)
BMEL 2016 Ergebnisse der Bundeswaldinventur 2012 *Technical Report* Bundesministerium für Ernährung und Landwirtschaft
BMEL 2018 Waldbrandstatistik der Bundesrepublik Deutschland für das Jahr 2018 *Technical Report* Bundesministerium für Ernährung und Landwirtschaft
BMEL 2019 Waldbrandstatistik der Bundesrepublik Deutschland für das Jahr 2019 *Technical Report* Bundesministerium für Ernährung und Landwirtschaft
Bonannella C, Hengl T, Heisig J, Wright M N, Herold M and de Bruin S 2022 Forest tree species distribution for Europe 2 2000–2020: mapping potential and realized 3 distributions using spatiotemporal Machine 4 Learning *PeerJ* **46** 28
Bouvier M, Durrieu S, Fournier R A and Renaud J-P 2015 Generalizing predictive models of forest inventory attributes using an area-based approach with airborne LiDAR data *Remote Sens. Environ.* **156** 322–34
Brown J K 1978 *Weight and Density of Crowns of Rocky Mountain Conifers* (*Intermountain Forest and Range Experiment Station, Forest Service*) (U.S. of Agriculture)
Cardil A, Monedero S, Schag G, de Miguel S, Tapia M, Stoof C R, Silva C A, Mohan M, Cardil A and Ramirez J 2021 Fire behavior modeling for operational decision-making *Curr. Opin. Environ. Sci. Health* **23** 100291
Chamberlain C P, Sánchez Meador A J and Thode A E 2021 Airborne lidar provides reliable estimates of canopy base height and canopy bulk density in southwestern ponderosa pine forests *Forest Ecol. Manage.* **481** 118695
Chuvieco E, Aguado I, Salas J, García M, Yebra M and Oliva P 2020 Satellite remote sensing contributions to wildland fire science and management *Curr. Forestry Rep.* **6** 81–96
Chuvieco E, Riaño D, Van Wagtendok J and Morsdof F 2003 Fuel loads and fuel type mapping *Wildland Fire Danger Estimation and Mapping - The Role of Remote Sensing* (*Series in Remote Sensing*) vol 4 (World Scientific Publishing Co. Pte. Ltd) pp 119–42
De Bruin S, Brus D J, Heuvelink G B M, Van Ebbenhorst Tengbergen T and Wadoux A M J-C 2022 Dealing with clustered samples for assessing map accuracy by cross-validation *Ecol. Inf.* **69** 101665
Dostálová A, Milenković M, Hollaus M and Wagner W 2016 Influence of forest structure on the Sentinel-1 backscatter variation - analysis with full-waveform LiDAR data *ESA Living Planet Symp.* p 9
Dubayah R *et al* 2020 The global ecosystem dynamics investigation: high-resolution laser ranging of the Earth's forests and topography *Sci. Remote Sens.* **1** 100002
Dubayah R, Hofton M, Bryan Blair J, Armston J, Tang H, and Luthcke S 2021a GEDI L2A elevation and height metrics data global footprint level V002 [Data set]
Dubayah R, Hofton M, Bryan Blair J, Armston J, Tang H and Luthcke S 2021b GEDI L2B canopy cover and vertical profile metrics data global footprint level V002 [Data set]
Duncanson L 2022 Aboveground biomass density models for NASA's Global Ecosystem Dynamics Investigation (GEDI) lidar mission *Remote Sens. Environ.* **20** 45
Erdody T L and Monika Moskal L 2010 Fusion of LiDAR and imagery for estimating forest canopy fuels *Remote Sens. Environ.* **13** 2
ESA 2023 Copernicus Sentinel data
EU, CLMS, EEA 2023 European Union, Copernicus Land Monitoring Service, European Environment *Agency: CLMS Data Access*
Ewald Fassnacht F, White J C, Wulder M A, Næsset E and Achim A 2024 Remote sensing in forestry: current challenges, considerations and directions *Forestry* **97** 11–37
Finney M A 1998 FARSITE: fire area simulator-model development and evaluation *Technical Report* RMRS-RP-4 U.S. Department of Agriculture, Forest Service, Rocky Mountain Research Station, Ft. Collins, CO
García M, Saatchi S, Casas A, Koltunov A, Ustin S, Ramirez C and Balzter H 2017 Extrapolating forest canopy fuel properties in the California rim fire by combining airborne LiDAR and landsat OLI data *Remote Sens.* **9** 394
GDI Thüringen 2023 Laserscanning - Daten des Thüringer Landesamtes für Bodenmanagement und Geoinformation
Geobasis NRW 2023 3D-Messdaten Laserscanning Nordrhein-Westfalen
GeoSN 2023 Laserscandaten des Landesamtes Geobasisinformation Sachsen
Gorelick N, Hancher M, Dixon M, Ilyushchenko S, Thau D and Moore R 2017 Google Earth Engine: planetary-scale geospatial analysis for everyone *Remote Sens. Environ.* **202** 18–27
Hansen M C *et al* 2013 High-resolution global maps of 21st-century forest cover change *Science* **342** 850–3
Haralick R M, Shanmugam K and Dinstein I'H 1973 Textural features for image classification *IEEE Trans. Syst. Man Cybern.* **SMC-3** 610–21
Healey S P, Yang Z, Gorelick N and Ilyushchenko S 2020 Highly local model calibration with a new GEDI LiDAR asset on Google Earth Engine reduces Landsat forest height signal saturation *Remote Sens.* **12** 2840

Heisig J, Milenković M and Pebesma E 2025 High-resolution canopy fuel maps based on GEDI: A foundation for wildfire modeling in Germany [Data set] (Zenodo) (https://doi.org/10.5281/zenodo.14622044)
Heisig J, Olson E and Pebesma E 2022 Predicting wildfire fuels and hazard in a central European temperate forest using active and passive remote sensing *Fire* **5** 29
Hermosilla T, Bastyr A, Coops N C, White J C and Wulder M A 2022 Mapping the presence and distribution of tree species in Canada's forested ecosystems *Remote Sens. Environ.* **282** 113276
Hermosilla T, Ruiz L A, Kazakova A N, Coops N C and Monika Moskal L 2014 Estimation of forest structure and canopy fuel parameters from small-footprint full-waveform LiDAR data *Int. J. Wildland Fire* **23** 224
Hiemstra P H, Pebesma E J, Twenhöfel C J W and Heuvelink G B M 2008 Real-time automatic interpolation of ambient gamma dose rates from the Dutch radioactivity monitoring network *Comput. Geosci.* **35** 11
Hijmans R J, Bivand R, Pebesma E and Sumner M D 2022 terra: spatial data analysis
Hoffrén R, Teresa Lamelas M, de la Riva J, Domingo D, Luis Montealegre A, García-Martín A and Revilla S 2023 Assessing GEDI-NASA system for forest fuels classification using machine learning techniques *Int. J. Appl. Earth Obs. Geoinf.* **116** 103175
Hudak A T, Bright B C, Pokswinski S M, Louise Loudermilk E, O'Brien J J, Hornsby B S, Klauberg C and Silva C A 2016 Mapping forest structure and composition from low-density LiDAR for informed forest, fuel and fire management at Eglin Air Force Base, Florida, USA *Can. J. Remote Sens.* **42** 411–27
Ilich A R 2020 GLCMTextures (available at: https://github.com/ailich/GLCMTextures)
IPCC 2014 Climate change 2014: synthesis report *Contribution of Working Groups I, II and III to the Fifth Assessment Report of the Intergovernmental Panel on Climate Change Core Writing Team)* ed R K Pachauri and L A Meyer (IPCC) Technical Report p 151
Jennings S, Brown N and Sheil D 1999 Assessing forest canopies and understorey illumination: canopy closure, canopy cover and other measures *Forestry* **72** 59–74
Kacic P, Thonfeld F, Gessner U and Kuenzer C 2023 Forest structure characterization in Germany: novel products and analysis based on GEDI, Sentinel-1 and Sentinel-2 data *Remote Sens.* **15** 1969
Kassambara A 2023 ggpubr: 'ggplot2' based publication ready plots
Keane R E, Burgan R and van Wagtendonk J 2001 Mapping wildland fuels for fire management across multiple scales: Integrating remote sensing, GIS and biophysical modeling *Int. J. Wildland Fire* **10** 301
Keane R E, Gray K and Bacciu V 2012 Spatial variability of wildland fuel characteristics in northern Rocky Mountain ecosystems *Technical Report* RMRS-RP-98 U.S. Department of Agriculture, Forest Service, Rocky Mountain Research Station, Ft. Collins, CO
Kuhn M 2021 Caret: classification and regression training
Lang N, Jetz W, Schindler K and Dirk Wegner J 2022 A high-resolution canopy height model of the Earth (arXiv:2204.08322)
Lanorte A *et al* 2001 Development of a European fuel map based on a novel classification suited to EU environments
LDBV 2023 Laserpunkte der Bayerischen Vermessungsverwaltung
Leite R V *et al* 2022 Large scale multi-layer fuel load characterization in tropical savanna using GEDI spaceborne lidar data *Remote Sens. Environ.* **268** 112764
LGB 2023 Laserscandaten der Landesvermessung und Geobasisinformation Brandenburg
Li W, Guo Q, Jakubowski M K and Kelly M 2012 A new method for segmenting individual trees from the lidar point cloud *Photogramm. Eng. Remote Sens.* **78** 75–84
Lin Pedersen T 2022 patchwork: the composer of plots
Linnenbrink J, Milá C, Ludwig M and Meyer H 2023 kNNDM: k-fold nearest neighbour distance matching cross-validation for map accuracy estimation *EGUsphere* **2023** 1–16
Loomis R M and Roussopoulos P J 1978 Estimating aspen crown fuels in northeastern Minnesota *Technical Report* North Central Forest Experiment Station, Forest Service, U.S. Dept. of Agriculture, Saint Paul
Lucrecia Pettinari M and Chuvieco E 2016 Generation of a global fuel data set using the fuel characteristic classification system *Biogeosciences* **13** 2061–76
Ludwig M, Moreno Martinez A, Hölzel N, Pebesma E and Meyer H 2023 Assessing and improving the transferability of current global spatial prediction models *Glob. Ecol. Biogeogr.* **32** 356–68
Lutes D C 2021 FuelCalc User's Guide (version 1.7) U.S. Department of Agriculture, Forest Service, Rocky Mountain Research Station
Mahoney M J, Johnson L K, Silge J, Frick H, Kuhn M and Beier C M 2023 Assessing the performance of spatial cross-validation approaches for models of spatially structured data (arXiv:2303.07334 [stat])
Marino E, Ranz P, Luis Tomé J, Ángel Noriega M, Esteban J and Madrigal J 2016 Generation of high-resolution fuel model maps from discrete airborne laser scanner and Landsat-8 OLI: a low-cost and highly updated methodology for large areas *Remote Sens. Environ.* **187** 267–80
Meyer H, Milá C, Ludwig M and Linnenbrink J 2023 CAST: 'caret' applications for spatial-temporal models
Meyer H and Pebesma E 2022 Machine learning-based global maps of ecological variables and the challenge of assessing them *Nat. Commun.* **13** 2208
Milá C, Mateu J, Pebesma E and Meyer H 2022 Nearest neighbour distance matching leave one out cross validation for map validation *Methods Ecol. Evol.* **13** 1304–16
Montero D, Aybar C, Mahecha M D and Wieneke S 2022 Spectral: awesome spectral indices deployed via the Google Earth Engine Javascript API *Int. Arch. Photogr. Remote Sens. Spatial Inf. Sci.* **48** 301–6
Moreno-Martínez Alvaro *et al* 2018 A methodology to derive global maps of leaf traits using remote sensing and climate data *Remote Sens. Environ.* **218** 69–88
Mullissa A, Vollrath A, Odongo-Braun C, Slagter B, Balling J, Gou Y, Gorelick N and Reiche J 2021 Sentinel-1 SAR backscatter analysis ready data preparation in Google Earth Engine *Remote Sens.* **13** 1954
Ole Ørka H, Dalponte M, Gobakken T, Næsset E and Theodor Ene L 2013 Characterizing forest species composition using multiple remote sensing data sources and inventory approaches *Scand. J. Forest Res.* **28** 677–88
Parkan M and Tuia D 2018 Estimating uncertainty of point-cloud based single-tree segmentation with ensemble based filtering *Remote Sens.* **10** 335
Pebesma E J 2004 Multivariable geostatistics in S: the gstat package *Comput. Geosci.* **30** 683–91
Pebesma E and Bivand R 2023 *Spatial Data Science: With Applications* (R. Chapman and Hall/CRC)
Potapov P *et al* 2021 Mapping global forest canopy height through integration of GEDI and Landsat data *Remote Sens. Environ.* **253** 112165
R Core Team 2023 *R: A Language and Environment for Statistical Computing* (R Foundation for Statistical Computing)
Reinhardt E, Lutes D C and Scott J H 2006 FuelCalc: a method for estimating fuel characteristics *Conf. Proc.* p 10

Riaño D 2003 Modeling airborne laser scanning data for the spatial generation of critical forest parameters in fire behavior modeling *Remote Sens. Environ.* **86** 177–86
Roberts D R *et al* 2017 Cross-validation strategies for data with temporal, spatial, hierarchical, or phylogenetic structure *Ecography* **40** 913–29
Rollins M G 2009 LANDFIRE: a nationally consistent vegetation, wildland fire and fuel assessment *Int. J. Wildland Fire* **18** 235
Roussel J-R *et al* 2020 lidR: an R package for analysis of airborne laser scanning (ALS) data *Remote Sens. Environ.* **251** 112061
Sánchez Sánchez Y, Martínez-Graña A, Santos Francés F and Mateos Picado M 2018 Mapping wildfire ignition probability using Sentinel 2 and LiDAR (Jerte Valley, Cáceres, Spain) *Sensors* **18** 826
Santoro M and Cartus O 2021 ESA biomass climate change initiative (biomass_cci): global datasets of forest above-ground biomass for the years 2010, 2017 and 2018
Schiefer F, Kattenborn T, Frick A, Frey J, Schall P, Koch B and Schmidtlein S 2020 Mapping forest tree species in high resolution UAV-based RGB-imagery by means of convolutional neural networks *ISPRS J. Photogramm. Remote Sens.* **170** 205–15
Schuldt B *et al* 2020 A first assessment of the impact of the extreme 2018 summer drought on Central European forests *Basic and Appl. Ecol.* **45** 86–103
Schwalb-Willmann J 2022 Basemaps: accessing spatial basemaps in R
Scott J H and Reinhardt E D 2001 *Assessing Crown Fire Potential by Linking Models of Surface and Crown Fire Behavior* (U.S. Department of Agriculture, Forest Service, Rocky Mountain Research Station) p 59
Seidl R, Schelhaas M-J, Rammer W and Johannes Verkerk P 2014 Increasing forest disturbances in Europe and their impact on carbon storage *Nat. Clim. Change* **4** 806–10
Senf C, Pflugmacher D, Zhiqiang Y, Sebald J, Knorn J, Neumann M, Hostert P and Seidl R 2018 Canopy mortality has doubled in Europe's temperate forests over the last three decades *Nat. Commun.* **9** 4978
Shimada M, Itoh T, Motooka T, Watanabe M, Shiraishi T, Thapa R and Lucas R 2014 New global forest/non-forest maps from ALOS PALSAR data (2007–2010) *Remote Sens. Environ.* **155** 13–31
Snell J A K and Little S N 1983 Predicting crown weight and bole volume of five Western hardwoods *Technical Report* PNW-GTR-151 U.S. Department of Agriculture, Forest Service, Pacific Northwest Forest and Range Experiment Station
Taccaliti F, Venturini L, Marchi N and Lingua E 2021 Forest fuel assessment by LiDAR data. A case study in NE Italy
Thonfeld F, Gessner U, Holzwarth S, Kriese J, da Ponte E, Huth J and Kuenzer C 2022 A first assessment of canopy cover loss in Germany's forests after the 2018–2020 drought years *Remote Sens.* **14** 562
Valavi R, Elith J, Lahoz-Monfort J J, Guillera-Arroita G and Warton D 2019 blockCV: An R package for generating spatially or environmentally separated folds for k-fold cross-validation of species distribution models *Methods Ecol. Evol.* **10** 225–32
Wadoux A M J-C, Heuvelink G B M, De Bruin S and Brus D J 2021 Spatial cross-validation is not the right way to evaluate map accuracy *Ecol. Modelling* **457** 109692
Wickham H 2016 *Ggplot2: Elegant Graphics for Data Analysis* (Springer)
Wickham H, François R, Henry L, Müller K and Vaughan D 2023a dplyr: a grammar of data manipulation
Wickham H and Henry L 2023 purrr: functional programming tools
Wickham H, Vaughan D and Girlich M 2023b tidyr: Tidy Messy Data
Wright M N and Ziegler A 2017 ranger: a fast implementation of random forests for high dimensional data in C++ and R *J. Stat. Softw.* **77** 1–17
Zanaga D *et al* 2021 ESA WorldCover 10 m 2020 v100 (available at: https://zenodo.org/record/5571936)